The fate of tidal flats across the world

Master Major Research Project

Source: European Space Agency

Name:	*Roland Weenink*		
Master:	*Science & Business Management (Utrecht University)*		
Student number:	*6013848*		
Supervisor (UU):	*Dr. Elisabeth Addink*	–	UU Geosciences
Supervisor (NIOZ):	*Prof. Dr. Tjeerd Bouma*	–	UU / NIOZ Geosciences
Daily supervisor:	*PhD. Tim Grandjean*	–	NIOZ Estuarine & Delta systems

Abstract
Forty percent of the human population lives within 100 km of the coast, and relies on it for their livelihood. One of the most prevalent coastal ecosystems in the world are tidal flats, which provide essential ecosystem services such as storm protection. However, tidal flat extent is on the decline, with 16% of all tidal flats already lost between 1984 and 2016. The underlying mechanisms leading to this decline are poorly understood. Studies have suggested suspended particulate matter (SPM) to be of influence in the changing morphology of tidal flats. To be able to remote sense SPM globally, turbidity is often used as a proxy. In this study, the relationship between turbidity change and a change in tidal flat morphology on a global scale between 1984 and 2013 is researched via remote sensing. The change in morphology of a tidal flat is define as a combination of both saltmarsh area change and elevation change. In 84.4% of the researched tidal flats, a negative correlation was found between turbidity and saltmarsh extent. However, no strong correlation between turbidity change and elevation change was found. Overall, this study found that a change in turbidity can explain part of the morphology change in tidal flats over time. Improvements to the method could result in more precise data on the correlation between turbidity change and elevation change and therefore help better understand the relationship between turbidity change and morphology change in tidal flats all over the world.

Layman's Summary
The most densely populated parts of the world are coastal regions. Forty percent of the human population lives here and relies on the coastal ecosystem services for their livelihood. The most common type of coast are tidal flats. Tidal flats are flats which are made up of silt, sand or mud and are frequently flooded due to tides. The three distinct zones of a tidal flat are a water channel, a mud flat and a saltmarsh. Tidal flats, and especially the saltmarshes of tidal flats are important for storm protection. However, tidal flats are disappearing, with 16% of all tidal flats in the world already lost since 1984. The reason behind this decline is not yet known. Studies suspect the amount of particles in the water of tidal flats to be related to this decline. The amount of particles in the water can be measured by looking at the degree of clarity of the water, which is called turbidity. This can also be done via satellite images, because the clearer the water is, the less infrared light it reflects. In this study, the change in turbidity, change in saltmarsh area and change in elevation of tidal flats worldwide will be assessed via satellite images. The change in saltmarsh area and change in elevation are used to determine the change in morphology of tidal flats. The morphology change can be used to see if a tidal flat is disappearing or not. If a change in turbidity can be linked to a change in morphology, a change in turbidity could be related to the disappearance of tidal flats worldwide. The results of this study show that in 84.4% of the tidal flats a decline in turbidity was linked to an increase in saltmarsh area. However, no direct link was found between a change in turbidity and a change in elevation of tidal flats. Therefore, only part of the morphological change in tidal flats can potentially be explained by a change in turbidity.

Acknowledgements
With this acknowledgement, I would really like to thank some people. The entirety of my major research project was done and written during the COVID-19 pandemic. This resulted in a lot of solitary work and concentration problems, especially during the writing phase of the project. Without the help of these people, it would have been much more difficult to eventually conclude this project and report.

First of, I would like to thank my daily supervisor, Tim Grandjean. He helped me during both the coding and writing part of this project. He was practically always available for answering my questions, providing me with ample amounts of feedback and for the quick discussion and thinking sessions on Teams. Sometimes those quick discussions turned into longer, fun conversations, which were very welcome due to the lockdowns at the time. Furthermore, Tim helped me learn python, since I had practically no previous experience with this programming language before starting this project. Lastly, I want to specifically thank Tim for creating the Digital Elevation Models and subsequent hypsometric curves used in this study.

Secondly, I would like to my other supervisors, Tjeerd Bouma and Elisabeth Addink. Tjeerd helped me by providing a plethora of ideas and with interpreting preliminary findings during the coding phase. I would like to thank Elisabeth for her help with narrowing down and defining the boundaries of this project, as well as helping me with the technical knowledge regarding remote sensing and providing feedback on written parts of the report. I would especially like to thank Elisabeth for getting me back on track during the writing phase. Without her help in scheduling and giving structure to the writing process, I would have taken much longer to actually finish the report.

Thirdly, I would like to thank my sister, Dana Weenink, who helped me with learning to code efficiently using python and enabled me to improve my skills further. Thank you for the hours you spent on looking over my code, helping me with improving it and guiding me through the steps to take when I got stuck.

Lastly, I would also like to thank my girlfriend, Fleur Colen, who read over and helped me formulate a lot of paragraphs. She was also there to keep me hydrated and fed when I was too immersed in writing and coding, to the point where I just forgot to drink and eat. She also ensured that loneliness did not become an issue during the lockdowns.

Table of Contents

Introduction

Worldwide more than 600 million people, approximately 10% of the total human population, live in the Low Elevated Coastal Zone (LECZ). This zone consists of connected land along the coast with a maximum elevation of 10 meters (Merkens et al., 2016). Furthermore, approximately 40% of the world population lives within 100 kilometres of the coast and rely on coastal and marine resources and ecosystem services (Neumann et al., 2015; United Nations, 2017). These numbers show how important coastal ecosystems are for the human population. One of the most prevalent coastal ecosystems in the world are tidal flats. These tidal flats fulfil multiple important ecosystem services, such as storm protection and food production (Costanza et al., 1997; Murray et al., 2019). They commonly have a high productivity and proved vital for many species, from micro- to macrofauna. Estuaries can function as nesting, breeding and migration stop-over grounds for many species of migratory birds, as well as breeding grounds for certain fish species (Deppe, 1999).

Tidal flats are intertidal environments consisting of sand, silt or clay, and are typically part of most tidally active estuaries (Healy et al., 2002). They form in areas where there is an abundant supply of fine-grained sediment and where the hydrodynamic forces, such as waves, are weaker than the tidal movements (Gao, 2018). Tidal flats are dynamic and generally grow in size if sediment transport is net landwards, and shrink if the sediment supply is cut off (Gao, 2018). Gradual and low slopes are characteristic for tidal flats and they are considered the typical form of muddy coasts (Healy et al., 2002). Going from highest to lowest elevation, they consist of a saltmarsh, mudflats and water (figure 1).

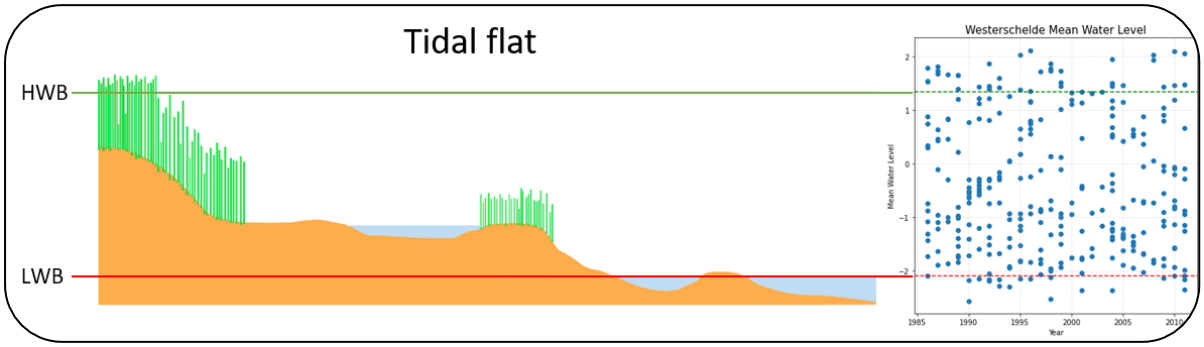

Figure 1: This figure shows a typical tidal flat morphology. The green line is the High-Water Boundary (HWB), meaning at the mean high the water level at that particular estuary reaches. At that point most of the saltmarshes (green area) are inundated. The Low-Water Boundary (LWB) is the red line. All parts of the tidal flat higher than the LWB are not inundated at low tide, including (parts of) the mudflats. Storm surges or spring tides can cause water levels to rise or fall beyond their respective Water Boundaries (adapted from Laengner et al. (2019)).

However, tidal flats and the ecosystem services they provide are under threat, with an approximate 16% of estuarine tidal flats already lost between 1984 and 2016 (Murray et al., 2019). There are multiple causes which contribute to this decline, including climate-change-driven sea-level rise, a reduction of sediment fluxes and coastal erosion (Murray et al., 2019; Passeri et al., 2015; Syvitski et al., 2009). Furthermore, anthropogenic processes such as an increase in coastal development or dams, put even more pressure on the ecosystems (Gao, 2018; Healy et al., 2002; Syvitski et al., 2005). One of the tidal flat ecosystem services under threat is storm protection. The saltmarshes of tidal flats provide wave attenuation, dampening the hydrodynamic energy of waves and tides, thereby providing a protective buffer effect for the coast (Fonsecal & Fisher, 1986; Ganthy et al., 2013; Verduin & Backhaus, 2000). With a decline in tidal flats, a decline in the protective buffer effect is expected and wave action will have a more direct impact on the coastline (Möller et al., 2014). Therefore, a decline in saltmarsh area is expected to lead to an increase in coastal erosion. This can already be observed in the Arcachon estuary, located on the South-western Atlantic coast of France. Here, a decline of approximately 33% of the meadows of *Zostera noltii* (dwarf eelgrass) between 1989 and 2007 was

observed by Ganthy et al., (2013) and consequently a switch from an accreting coast to an eroding coast in the 1970s was measured by (Castelle et al., 2018). However, this type of precise data to assess the status of estuaries worldwide is lacking, which makes quantifying the overall threat and extent of this decline difficult (Murray et al., 2019).

In order to restore and protect the estuarine flats against the threats they face, the causal underlying mechanism of the tidal flat decline needs to be understood. However, the common denominator and measurable factor of all the threats is difficult to determine. One potential underlying mechanism linked to the formation or shrinkage of tidal flats is a decline in sediment influx (Willemsen et al., 2022). This can partly be seen in the Yangtze river, where the building of dams has drastically decreased the sediment discharge to the coast, leading to a decline in sedimentation rates of the coastal environment (Yang et al., 2011). Another example is the Delta works in the Netherlands, which is the main cause for the decrease in sediment fluxes in the Oosterschelde, potentially causing the tidal flats to slowly decline in elevation and disappear into the ocean (van Maldegem & van Pagee, 2005). Furthermore, the estuary of Chwaka located in the island of Zanzibar, Tanzania, experiences high sediment transport variation due to the presence of strong tidal currents (Gullström et al., 2006). These changes in sediment are linked to large changes in emergent aquatic vegetation (saltmarshes) in Chwaka over time (Gullström et al., 2006). However, the direct relation between these sediment flow changes and the extent of the saltmarsh is unknown. Knowing these changes in sediment concentration over time and its effects for estuaries worldwide could potentially give indication to the future trajectories of tidal flats.

The trajectories of tidal flats could be better understood if the morphodynamics behind these tidal flat trajectories can be accurately determined (Hibma et al., 2004). However, there has been speculation whether tidal flats are in morphological equilibrium rather than having trajectories, some stating that continuous changes to the tidal flat indicate that there is no equilibrium present (Dronkers, 1986). Others argue that equilibrium can be found at a smaller scale in tidal flats (van der Wegen et al., 2008; Van Der Wegen & Roelvink, 2008). It is more likely that estuaries and tidal flats are in a morphodynamic equilibrium, meaning disturbances will eventually revert back to the original steady-state, or once threshold values are reached, impose a new steady state (Dam et al., 2016; Hu et al., 2015). If estuaries and their tidal flats are in a morphodynamic equilibrium, a long-term trajectory of the tidal flat can still be present, if the threshold to form a new steady state is repeatedly reached over a long time period. For example, a tidal flat could be relatively stable, but every 15 years the lower threshold of the determining variable is reached and a new steady-state is formed around the lower variable. This would mean there is a morphodynamic equilibrium, while also showing a declining trajectory in the long-term. However, as stated before, the variables which affect these potential trajectories are complex and difficult to determine and global-scale data on the change of tidal flats through time is not present (Murray et al., 2019). Furthermore, parameters such as the tidal difference (Dronkers, 1986), the bathymetry of an estuary (Pritchard & Hogg, 2003) and the cross-shape, either concave or convex (Kirby, 2000), are all said to also affect the trajectory of a tidal flat. However, these parameters are difficult to determine for estuaries on a global scale. One variable which solely might give an indication towards the trajectory of the tidal flat, is the estuary sediment concentration (Liu et al., 2021; Murray et al., 2019).

The collection of sediment concentration data is laborious, requires field studies and sample collections on site (Halper & McGrail, 1988). Consequently, the turbidity of the water column is frequently used as a proxy of sediment concentration (Bright et al., 2018). Turbidity is an optical measure of clarity of water, which is strongly affected by the sediment concentration. Turbidity is given in Formazin Nephelometric Units (FNU) and conveys more data than just the sediment concentration. Turbidity encompasses all suspended particles in the water column, including microscopic organisms, such as phytoplankton (Kitchener et al., 2017). Turbidity can be measured and

monitored more easily than sediment concentration data through the use of remote sensing and is referred to as a measurable proxy for suspended particulate matter (SPM) (Bright et al., 2018; Dogliotti et al., 2015; Gippel, 1995).

For a global-scale study, the method of acquiring the turbidity data needs to be a uniform method, providing valid data from sites all across the world. As mentioned before, the collection of turbidity data can more easily be accomplished than the collection of SPM. However, standard turbidity data collection generally still requires data to be collected on site. Most turbidity data is collected by taking a water sample in the field or through the use of installed water quality sensors (Myre et al., 2006; USGS, n.d.-c), and using one of the accepted turbidity standards: USEPA Method 180.1, ISO 7027 and GLI Method 2 for the calculations (Andrew Ziegler, 2002; Kitchener et al., 2017). However, since all of these methods require ground equipment or *in-situ* data collection, they become impractical when conducting larger scale studies. Furthermore, the exact same methodology needs to be applied to each, separate estuary data collection. For a large scale, global study, this requirement makes *In-situ* data collection impractical. Turbidity can also be collected through the use of remote sensing, by using satellite surface reflectance data to calculate turbidity as described by Nechad et al. (2010) and Kalele (2019). However, this method still requires calibration coefficients for each location, which are based on field studies of the given site. Since field studies of every estuary cannot be expected to be uniformly collected in a global study, this method still has its shortcomings.

To overcome the burden of requiring field studies for turbidity data collection, Dogliotti et al. (2015) proposed a single turbidity retrieval algorithm which is valid worldwide and not dependent on region-specific calibration coefficients. Dogliotti et al. (2015), tested the retrieval algorithm on five different sites, the North Sea, the Scheldt, Gironde, French Guyana and Río de la Plata. The algorithm performed within 12% to 22% of *in-situ* data of these five sites (Dogliotti et al., 2015). The overall mean relative error and bias of the retrieval algorithm was found to be respectively 13.7% and 4.8% (Dogliotti et al., 2015). For a global scale study, with no calibration necessary, these results are promising.

Turbidity can potentially be an underlying cause for a trajectory of a tidal flat, but the trajectory itself is determined by the change in morphology through time. The morphology of tidal flats consists of many different parameters and is influenced by many processes (Gao, 2018; Robins & Davies, 2010). The complete morphology of a tidal flat is very complex, touching upon hydrodynamics, sedimentology, bathymetry, tidal action and many more morphodynamics (Friedrichs, 2012; Gao, 2018; Robins & Davies, 2010). However, some measurable parameters can serve as a proxy for tidal flat morphology, such as a change in elevation or saltmarsh extent (Friedrichs, 2012; Healy et al., 2002).

To measure a change in tidal flat morphology through a change in elevation globally, heightmaps can be used. Heightmaps can be created through remote sensing. Tong et al. (2020), describes a method using the change in waterline through time to determine the change in eleveation of a tidal flat, called the waterline extraction method. This method can also be used to determine the what part of the slope of a tidal flat has changed.

Another part of the change in morphology can be studied through area classification methods of satellite images, as described by Laengner et al., (2019). They devised a classification method to detect trends in saltmarsh habitat area change across Europe. This is achieved by using an unsupervised classification system (Leangner et al., 2019). Through the use of this method, the extent of saltmarshes, mudflat and water area can be mapped and the change in size of these areas through time can be visualised. This can give insight into the way the morphology of a tidal flat or estuary changes in responds to a changing environment. The combination of elevation change and the extent of certain habitats, such as saltmarshes, essentially serves as a proxy for the morphological change of

a tidal flat. Using this in conjunction with detecting a change in turbidity could give insight in the relation between these variables.

To assess if a change in turbidity affects the morphology of tidal flats, the following research question will be answered:

How does a change in turbidity over time influence the morphology of a tidal flat in an estuary and can this be measured globally?

- *What is the change in turbidity for estuaries worldwide?*
- *What is the change in saltmarsh area for estuaries worldwide?*
- *What is the change in elevation for estuaries worldwide?*

Method

To calculate the turbidity and morphological change of estuaries worldwide, remote sensing is used. The satellite data used in this study is Landsat surface reflectance data, provided by NASA and the United States Geological Survey (USGS). Landsat data is used due to the repeat cycle of 16 days, a relatively large spatial coverage of 185x185km and the spatial resolution (USGS, n.d.-a). Solely the surface reflectance data of Landsat 5 is used, as opposed to other (Landsat) satellites or a combination of different Landsat satellites. The usage of only Landsat 5 data is based on it having the longest period of continuous service, from 1984 to 2012, as well as having a spatial resolution of 30x30m (Earth Engine, n.d.). Landsat 3 or older Landsat satellites have a lower spatial resolution, and newer Landsat satellites have a shorter period of continuous service, making Landsat 5 the best fit for this study. A combination of Landsat 4, 5, 7 and 8 could also be used to increase the period of service, since they all provide the same spatial resolution of 30x30m. However, the usage of multiple satellites introduces a margin of error into the surface reflectance data. This is due to every Landsat satellite having slightly different sensors. Furthermore, only the Tier 1 surface reflectance data of Landsat 5 is used. The Tier 1 surface reflectance data consists of Landsat 5 images with only the highest available data quality and is atmospherically corrected, meaning most radiometric noise and atmospheric influences are filtered out (Young et al., 2017).

Data

A plethora of tools is used to access and analyse the Landsat 5 Tier 1 surface reflectance data and determine the turbidity and the land cover, as well as monitor the change of these parameters through time for each estuary. The python-based Google Earth Engine (GEE), and subsequent compatible packages, were used to analyse and access the surface reflectance data. One of such packages is GeeMap, which is a package for interactive mapping of satellite imagery and geospatial datasets (Wu, 2020). The Google Earth Engine was used, not only for its multitude of helpful tools, but also due to its direct access to the Earth Engine Data Catalog (Google Earth Engine, n.d.), meaning the relatively large Landsat 5 images could be accessed directly, within the cloud servers. To accommodate this, most of the python code was developed and run from a Google Colab environment, thereby making use of the google servers' processing power and data storage.

Data correction

To increase the accuracy of the later calculations, first the Landsat surface reflectance data is filtered based on image quality and cloud cover. The Landsat 5 Tier 1 surface reflectance images contain this information in their metadata and can therefore be filtered based on it. The image quality is ranked on a scale of 0 to 9, wherein 9 is the best. The image cloud cover is given as a percentage value. All images with an image quality lower than 6 and with a cloud cover higher than 60% are filtered out.

Pre-processing

After this step, all remaining surface reflectance data images of Landsat 5, collected between 1986 and 2012, are sorted into nine, 3-year image collections, as is commonly done for estuary data (Laengner et al., 2019). Binning the images to image collections ensures pixel data availability in an estuary. These image collections, are then subjected to a cloud mask function based on the quality assessment band provided by GEE (USGS, n.d.-b). This function masks the remaining clouds in the image collection pixelwise based on the pixel quality metadata. The data of every pixel in the image collection is then combined into a single image using a median reducer. The median reducer is used to reduce noise in the image. It does this pixel-wise by taking the values of neighbouring pixels of a pixel, calculating the median of these values for every image in the image collection and assigning the median value to the pixel if the original value is too much of an outlier compared to the pixel value in the other images. Due to the median reducer, a large outlier will not skew the image significantly. A simplified visual representation of this process can be seen in figure 2. The reflectance data in the

images is stored in a native integer raster format, used by NASA / USGS. To correct for this and make the data workable, it is divided by 10.000.

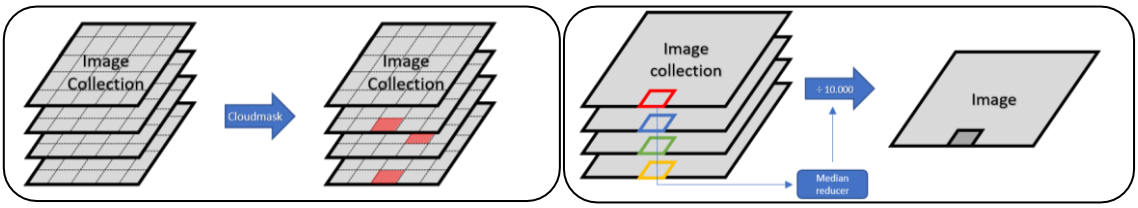

Figure 2: The 3-year image collection is subjected to a pixelwise mask function to increase the overall pixel quality of the collection (left). The image collection is then reduced into a single image, with every pixel in the resulting image containing the median data of the previous image collection pixels at that specific location.

Processing

Before specific calculation are made, first the areas of interests need to be determined. The areas of interest are estuaries with tidal flats, including saltmarshes. These estuaries (figure 3) were gathered from the Protected Planet database and from NATURA-2000 for the EU estuaries (Natura2000, n.d.; *The World's Protected Areas*, n.d.). If available, the base estuary shapefiles were used. However, in some cases, the shapefiles were manually edited to remove man-made structures such as agricultural fields and embanked areas. For some estuaries no base shapefiles were available. These shapefiles were manually created using QGIS. This resulted in 45 estuaries worldwide. The shapefiles are loaded into the GEE python environment and converted to an Earth Engine compatible file format. The image collections are then geographically clipped to only contain pixels which fall into the specified shapefile.

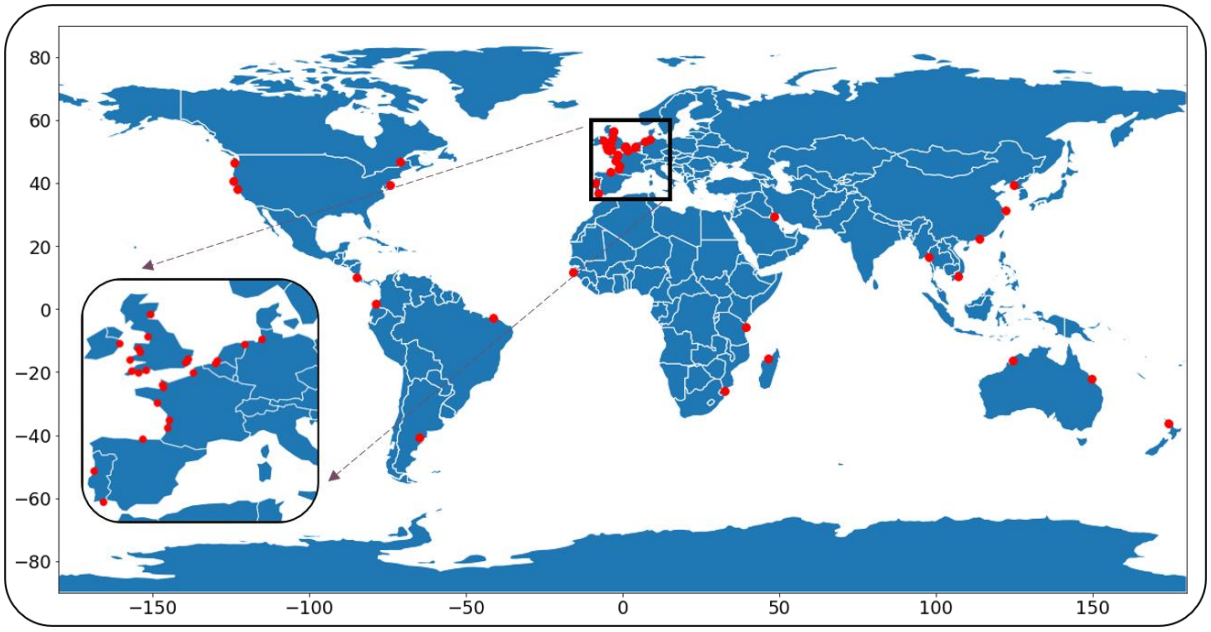

Figure 3: All 45 estuary locations used in this study. Most of the locations are in Europe due to a combination of a higher data availability as well as good coastal conditions for estuary and tidal flat formations.

Area classification

Before the turbidity of the estuaries can be calculated, first the land cover of every pixel needs to be determined to ensure turbidity data is only collected from water. There are multiple methods to do this. The method of choice is an adaptation of the unsupervised decision tree classification method (Laengner et al., 2019). The basic premise of this method is determining the land cover, either water, mudflat or saltmarsh, for each pixel through the use of the Normalized Difference Vegetation Index (NDVI) and the Normalized Difference Water Index (NDWI), and setting certain thresholds. An

unsupervised decision tree method is used because no accurately labelled dataset of all estuaries exists currently.

The first step is calculating the NDVI for every pixel in the image. This is done using a python NDVI function, which follows the standard NDVI calculations (figure 4). Tidal flats are known to accommodate (green) algae mats, which could be identified as vegetation when using a low NDVI threshold (Jaewon, 2005; Lee et al., 2005; Won et al., 2005). Therefore, NDVI threshold is set at 0.3 as to prevent algae mats from being classified as saltmarshes, thereby skewing the estuary land cover ratio more towards saltmarsh (Laengner et al., 2019; Sun et al., 2016; van der Wal et al., 2010). Since a median reducer is used to create the single image from an image collection spanning 3 years, the pixels which are classified as saltmarsh through this method are saltmarsh in at least the 50th percentile of the original images.

a $$NDWI = \frac{Green - NIR}{Green + NIR}$$

b $$NDVI = \frac{NIR - Red}{NIR + Red}$$

Figure 4: The formula for a) Normalized Difference Water Index (NDWI) and b) Normalized Difference Vegetation Index (NDVI) wherein NIR stands for Near infrared (Dogliotti et al., 2015; Szabó et al., 2016).

Determining what pixels in an estuary are mudflat is done through the use of masking pixels with both NDVI and NDWI value thresholds (Figure 4). First a new reduced image is created from the cloud masked image collection. This time a 25th percentile reducer is used instead of a median reducer, as to not underrepresent mudflat, due to its nature of being inundated. During inundation, mudflats will be classified as 'water'. In this image, all pixels previously classified as saltmarsh are masked. The NDWI values of all remaining pixels are calculated. All pixels with a NDVI value lower than the 0.3 threshold and an NDWI value higher than the 0.0 threshold are classified as potentially mudflat. The 'potentially mudflat' pixels are then checked on whether neighbouring pixels are also classified as mudflat using the 'ConnectedPixels' GEE function. If multiple potentially mudflat pixels are connected, they are then classified as mudflat. This is done as to limit the effect of random mudflat pixels in the middle of the water column, which might occur due to the water potentially being very turbid in estuaries and tidal flats. However, this method of preventing water pixels being defined as mudflat pixels is not foolproof, and if enough images are taken during times of peak turbidity, water pixels can potentially still be wrongly classified as mudflat.

After these two steps, all pixels which are classified as mudflat and saltmarsh are masked. All remaining pixels with a NDWI value greater than the 0.0 threshold are classified as water. The 'potentially mudflat' pixels which have no neighbouring mudflat pixels and connect to a water pixel are also classified as water using the GEE blend function. This method assures that only the channel in tidal flats is classified as water.

Lastly, to go from number of pixels to an area in km^2, a calculation needs to be done. The number of pixels of a land cover type is multiplied by the spatial resolution of Landsat 5 which is 30x30m = 900m^2. However, the inclination of the satellite also needs to be corrected for, resulting in a mean spatial resolution of 550m^2. This results in the following equations to go from number of pixels to area in km^2:

$$Area\ (m^2) = Pixel\ count * 550m^2$$

$$Area\ (km^2) = {Area\ (m^2)}\Big/{1{,}000{,}000}$$

The method applied here differs from the method by Laengner et al. (2019), in that the shapefiles used here already exclude any terrestrial vegetation. In the original method, first an extra masking of terrestrial vegetation is applied based on addition land cover information, because terrestrial vegetation would otherwise be classified as saltmarsh. Since the estuaries in this study are all over the world, this additional land cover information would not always be available. Therefore, excluding terrestrial vegetation would not be equally applied on every estuary, thereby introducing a bias in the data towards more saltmarsh in areas with lower data availability.

Turbidity calculation

Turbidity calculations normally require calibration coefficients based on the specific parameters pertaining to the study site at hand. Since this is a study of estuaries around the world, these calibration coefficients cannot always be calculated, seeing as the *in-situ* data cannot always be collected. Therefore, the turbidity calculations in this study are based on a single turbidity retrieval algorithm as proposed by Dogliotti et al. (2015) (Figure 5). This single algorithm is based on a turbidity retrieval algorithm by Nechad et al. (2010) and uses two calibration coefficients A_t and C_t. There are only two different values for these calibration coefficients depending on whether the study site has high or low turbid water (Figure 6). The values for the calibration coefficients are taken directly from Nechad et al. (2010) and Dogliotti et al. (2011). Both sets of calibration coefficient values have been calibrated with *in-situ* data and are specifically chosen to be used as a generalised fit for most estuaries around the world (Dogliotti et al., 2015; Nechad et al., 2010).

$$T = \frac{A_T^{\lambda}\rho_w(\lambda)}{(1-\rho_w(\lambda)/C^{\lambda})} \quad [\text{FNU}]$$

T = Turbidity
A_T = Reflectance-dependent calibration coefficients
C = Reflectance-dependent calibration coefficients
ρ_w = Water reflectance
λ = wavelength

Figure 5: The Remote sensing turbidity (T) retrieval algorithm as described by Nechad et al. (2010). A description of the symbols and notations is also provided (Dogliotti et al., 2015; Nechad et al., 2010). Adapted.

λ (nm)	A_T	C_T
645	228.1	0.1641
859	3078.9	0.2112

Figure 6: The two sets calibration coefficient values for low turbid waters (645 µm) and high turbid waters (859 µm) (Dogliotti et al., 2011; Nechad et al., 2010).

The surface reflectance data from the Landsat 5 Tier 1 images consists of different reflectance values depending on what band or wavelength is used. The surface reflectance (P_w) of two bands or wavelengths are used in the single retrieval algorithm (Dogliotti et al., 2015). These two bands are the Red band (0.63 - 0.69 µm) and the NIR or Near infrared band (0.77-0.90 µm) (Earth Engine, n.d.). The near infrared band is most sensitive and accurate in high to medium turbid waters, whereas the accuracy of the red band is highest in low turbid waters (Dogliotti et al., 2015). The distinction between the two different bands is made to more accurately calculate the turbidity in both low and high turbid areas (Dogliotti et al., 2015). According to Dogliotti et al. (2015), the NIR-band loses sensitivity at waters with an approximate turbidity of 15 FNU or lower. The sensitivity of the red band is higher at these turbidity levels. Dogliotti et al. (2015) suggested a distinction to be made based on the surface reflectance value of the red band. This distinction is made to assure accurate turbidity calculations in both low and high turbidity waters. This distinction leads to the following three categories:

- Category 1: Pixels with a red band surface reflectance value lower than 0.05.
- Category 2: Pixels with a red band surface reflectance value between 0.05 and 0.07.
- Category 3: Pixels with a red band surface reflectance value higher than 0.07.

Before calculating the overall turbidity of the estuary, all pixels are sorted in these three categories. The turbidity calculation of all pixels sorted into category 1 or category 3 follows the standard single algorithm, wherein the surface reflectance value of red band and the NIR band is used respectively (Figure 5). However, in case only the red band or NIR band is used for the pixels of category 2, the accuracy of the turbidity calculation is poor. The pixels of category 2 fall into a transition zone, which can be best described as medium turbidity.

To accurately calculate the turbidity of the pixels in the transition zone, both the red band and NIR band surface reflectance need to be used. To accomplish this, first a linear weighting function is used (Figure 7). This weighting function, derived from Dogliotti et al. (2015), linearly aligns all pixels on a scale from 0 to 1 based on their red band reflectance value. As an example: If a pixel has a red band surface reflectance value of 0.058, the weight assigned to this pixel would be 0.4.

$$w = \frac{(p_{w_{red}} - 0.05)}{0.02}$$

Figure 7: The linear weighting function as described by Dogliotti et al. (2015).

After the weighting function, the turbidity of every pixel is calculated through the use of the single turbidity retrieval algorithm twice. Once using the surface reflectance and corresponding calibration coefficient of the red band and another time using the NIR band.

Lastly, the definitive turbidity of the pixel is calculated using a blending function (figure 8). This blending function calculates the turbidity based on the red band turbidity, the NIR band turbidity and the 'weight' of the pixel. The weight of the pixel effectively functions as a ratio, deciding how much of the pixel's turbidity is dependent on the red band and the NIR band. The weight therefore effectively functions as a ratio, deciding how much of the pixel's turbidity is calculated through the use of either the red or NIR band surface reflectance. After the turbidity has been calculated, to assess whether an estuary can be considered a high turbid or low turbid estuary, the median value of nine turbidity values of each estuary is taken. In FNU terms, waters are generally considered to have high turbidity at approximately 23 FNU (20FNU +- 10% to account for measurement inaccuracies) (Dogliotti et al., 2015; Klein et al., 2011; Rudorff et al., 2018; Weiffen et al., 2006). The median value is taken rather than the average, to account for outliers. An average of a series of values is more dominated by outliers than the typical values than a median.

$$T = (1 - w) \cdot T_{red} + w \cdot T_{NIR}$$

Figure 8: The blending function, wherein 'w' is the weight, T_{red} is the calculated turbidity using the red band and T_{NIR} is the calculated turbidity using the NIR band (Dogliotti et al., 2015).

Change in Morphology

A spearman correlation test is performed to assess the correlation between a change in turbidity through time and a change in saltmarsh area through time. This correlation can give an indication to whether a change in saltmarsh area could partially be correlated to a change in turbidity. If there is a correlation between turbidity change and saltmarsh area change, it strengthens the narrative that a change in turbidity affects saltmarshes and therefore the morphology of an estuary.

Hypsometric curves

Hypsometric curves were created based on Digital Elevation Models (DEMs) or heightmaps of every estuary in this study. These heightmaps and in turn hypsometric curves are made using the waterline extraction method, where a time series of satellite images are taken (Koopmans & Wang, 1994; Tong et al., 2020). The satellite images are taken at varying water levels, enabling accurate mapping of the waterline, thereby facilitating the creation of DEMs (Bishop-Taylor et al., 2019; Tong et al., 2020). These DEMs are made for the first period and the last period. By comparing the hypsometric curve of the first period with the hypsometric curve of the last period, a change in morphology can be easily spotted. The hypsometric curve makes it possible to see at what elevation level a change occurs.

Automatic determination

These hypsometric curves can be analysed to show the change in area between the first and the last period per elevation level. For example, if more erosion than accretion occurs at the higher elevation, but more accretion than erosion occurs at the lower elevation of an estuary, the estuary is determined to be 'Flattening Accreting'. There are 6 automatically detectable categories an estuary can be classified as: 'Erosion', 'Steepening Erosion', 'Flattening Erosion', 'Accretion', 'Steepening Accretion' and 'Flattening Accretion'. A tool is written to make this distinction automatically, called the hypsometric tool.

Another correlation between the change in turbidity and the estuary being either accreting or eroding is also determined. If the turbidity of an estuary has a positive trend through time and the hypsometric curve shows accretion, they are positively correlated and vice versa. If no real accretion or erosion can be found, no correlation can be found.

Statistical justification

The Landsat 5 images are taken at approximately the same time every day. Due to only Tier 1 images being used and additional images being filtered out beforehand, a lot of images are taken out in this study. This leaves less images per 3-year period to work with, thereby increasing the chances of introducing a bias due to data collection instead of actual statistical significance in the results. To counter this, the mean water level at the time each image is taken, is collected through the use of worldtides.info API, an API which checks the tidal datum based on coordinates (Worldtides, n.d.). To assess whether the used and collected data, do not introduce any biases, an index of dispersion is calculated over the image collection times and dates, and at what tide. The index of dispersion checks whether clustering occurs during data collection and is calculated over the Julian day of each image collection, on the date of the image collection and on the tidal datum at which each image in an estuary collection was made. By looking at the Julian day, a potential bias towards seasons can be spotted. The index of dispersion for the dates, show if there is a bias in data collection through the entire collection period. The dispersion index is calculated by taking the variance and dividing it by the mean: $D = \frac{\sigma^2}{\mu}$. The closer the dispersion index value is to 1, the less clustered or over-dispersed a dataset is.

Furthermore, the total amount of image per period per estuary is checked. If a certain period has significantly less images when compared to another period, the results of the calculations could be

caused by the difference in image counts. The difference in image counts could cause outliers to not be filtered out as effectively by taking the mean of each image, thereby introducing data skew.

Lastly, the results of four different estuaries will be discussed in this study. Which four estuaries will be used is based on the level of change over time in turbidity as well as the direction of said change and the direction of the morphological change, indicated by the change in elevation. elevation is chosen as the morphological indicator to base this choice on instead of saltmarsh area change, due to elevation also affecting the area of saltmarsh in an estuary (van der Wal et al., 2008). This should result in these four types of estuaries:
An estuary with

- An increase in turbidity over time and an increase in elevation
- An increase in turbidity over time and a decrease in elevation
- A decrease in turbidity over time and an increase in elevation
- A decrease in turbidity over time and a decrease in elevation

The results of the other estuaries are added in the appendix.

Results

Since the method used in the python script remains the same for every estuary worldwide, a few estuaries around the world are chosen to be shown here, and act as a representation of the other estuaries. The estuaries of which the results are shown are: Arcachon, Saint Michel, Westerschelde, Lawrence and Mottoma (Figure 9). Out of all estuaries, four are chosen based on their turbidity and morphological changes. In addition to these four, the Westerschelde is added in the results due to it being one of the most actively researched estuarine areas in the world. Furthermore, the Westerschelde is the estuary which the method was tested on and the script was validated on.

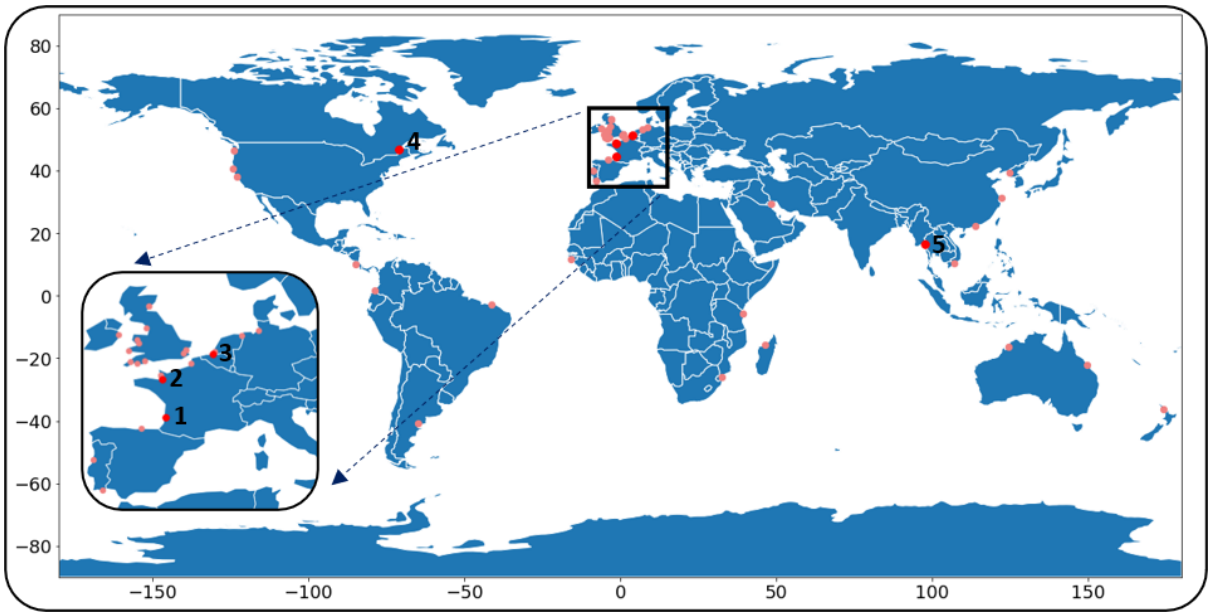

Figure 9: The location of the estuaries used in the Results are shown in Red. The other estuaries used in this study are shown in light red. 1 = Arcachon, 2 = Saint Michel, 3 = Westerschelde, 4 = Lawrence and 5 = Mottoma.

Arcachon

Area classification

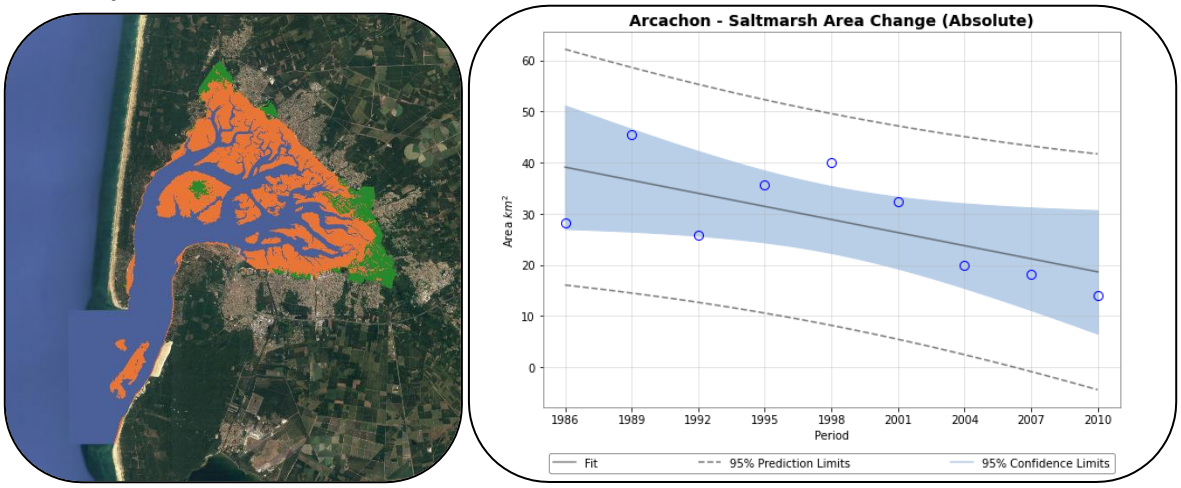

Figure 10: Arcachon, an estuary in the Southwest of France. The different colours indicate the different land cover types as per 2013 (Green = Saltmarsh, Brown = Mudflat) (left image). The right figure shows change in saltmarsh area in the Arcachon estuary between the periods 1986 and 2013.

The saltmarsh area of Arcachon (Figure 10) in the first period totals approximately 28.3 km^2. In the period 2010 – 2013 this has significantly decreased to a total square km area of approximately 14.1, which was also the lowest measured saltmarsh area in Arcachon during this study. The largest saltmarsh area was measured in the period 1989 – 1992, totalling an area of 45.5 km^2. The saltmarsh area decline of Arcachon has a mean slope of -1.86% per year.

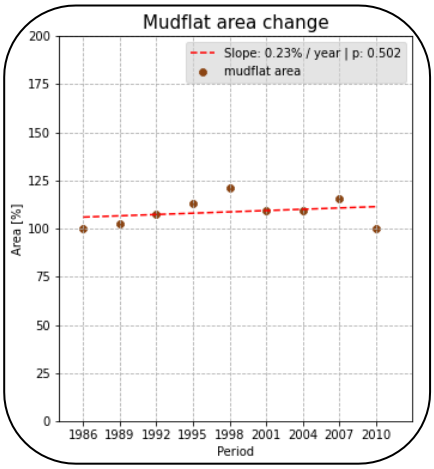

The mudflat area of Arcachon through time has an approximate change through time of 0.23% per year. The linear slope as seen in figure 11 is however not significant when a linear regression test is applied.

Figure 11: The mudflat area change between 1986 and 2013 in the Arcachon estuary. The rate of change (slope) is shown with the red line. The linear regression has a p-value of 0.502.

Turbidity calculations

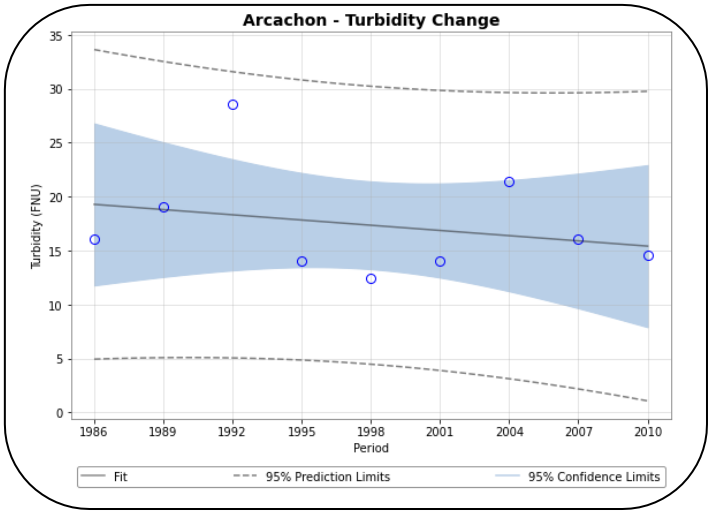

Figure 12: The turbidity calculations over pixels of the water channel of Arcachon estuary for the period 1986-1989 to 2010-2013.

The turbidity calculations for Arcachon show a slight decline in turbidity through time (Figure 12). The turbidity in the first period was 16.1 FNU whereas the last period has a turbidity of 14.6 FNU. The mean decline of the turbidity in Arcachon is -0.16% / year. This decline is somewhat skewed to the upside due to an outlier of 28.5 FNU in the period 1992-1995, being the highest measured turbidity for Arcachon over the study period. The lowest measured turbidity value was 12.4 FNU in the period 1998-2001. The standard deviation of the Arcachon turbidity measurements is 5.0, with a range of 16.1 FNU. However, if the outlier of 28.5 FNU is excluded, the standard deviation lowers to 2.9 and the range changes to 9.0 FNU.

Change in Morphology

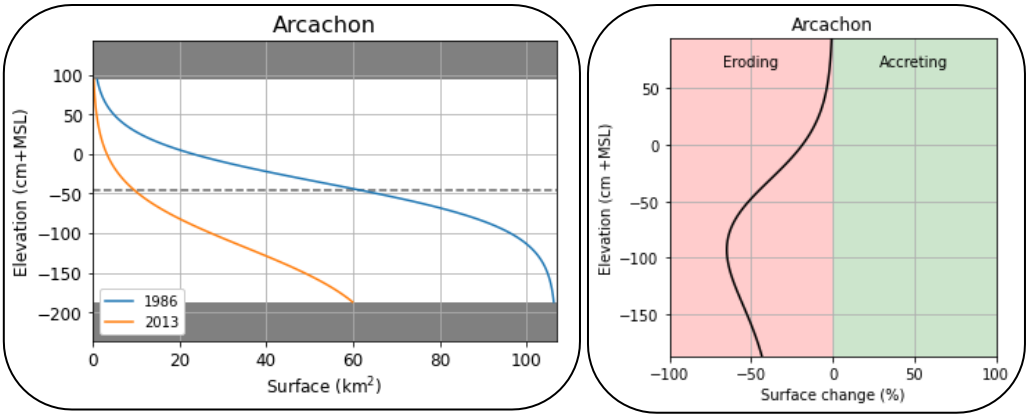

Figure 13: The left figure shows the hypsometric curve of Arcachon. The grey bars indicate the elevation limits, no surface change is detected beyond those values. The right image shows an automatic interpretation of the hypsometric curve with regards to morphology change by the hypsometric tool.

Looking at the hypsometric curve, Arcachon shows a large decrease in surface area, particularly in the low elevation levels (Figure 13). This indicates that the tidal flat of Arcachon is eroding, with a potential steepening effect, seeing as the surface change in the lower elevation levels is more significant than in the higher elevation levels.

The spearman correlation between the saltmarsh change through time and the turbidity change through time of Arcachon is -0.300 ($p = 0.4328$). There is no significant correlation between the decline of saltmarsh and the slow decline in turbidity in Arcachon.

Lawrence

Area classification

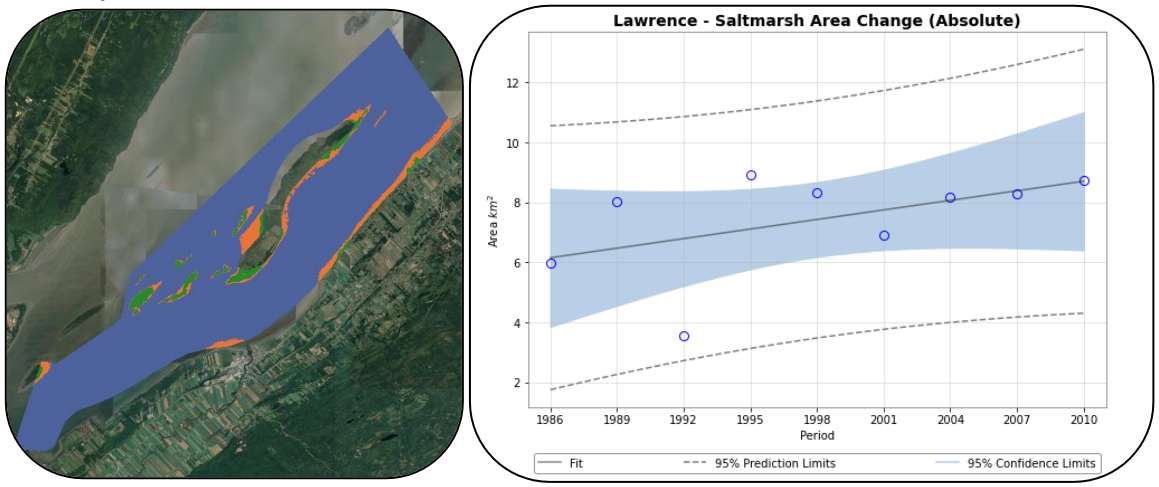

Figure 14: Lawrence is an estuary fed by the Saint Lawrence River, near Quebec, Canada. The different colours indicate the different land cover types as per 2013 (Green = Saltmarsh, Brown = Mudflat) (left image). The right figure shows change in saltmarsh area in Lawrence estuary between the periods 1986 and 2013.

In the Lawrence estuary, an increase from 6.0 km^2 saltmarsh area in the period 1986-1989 to 8.7 km^2 saltmarsh area in the period 2010-2013 was observed (Figure 14). The saltmarsh area of Lawrence increased through time with an approximate 1.78% / year. However, there are some significant outliers present, namely the saltmarsh area in the period 1992-1995. This was also the period with the lowest measured saltmarsh area in Lawrence during the study period. The saltmarsh area calculated over that period is 3.6km^2, or an approximate decline of 40% relative to the first period. The largest saltmarsh area was measured the following period with a saltmarsh area of 8.9 km^2.

Turbidity calculations

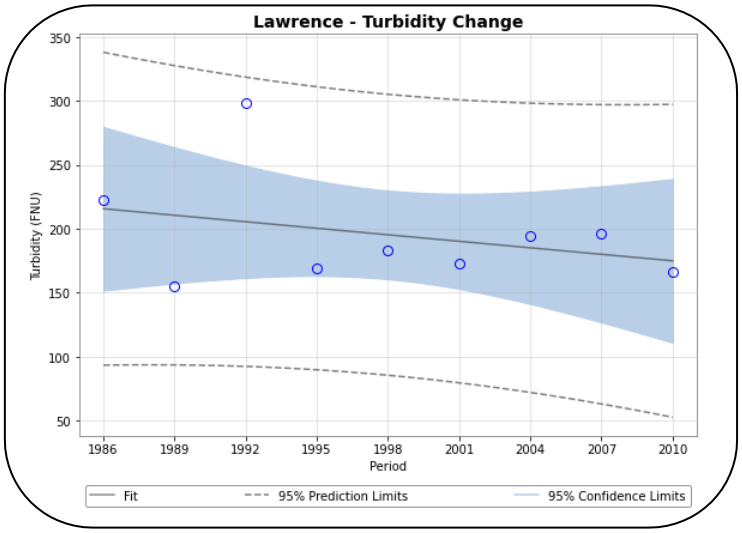

Figure 15: The results of the Lawrence estuary turbidity calculations are shown in this figure.

Lawrence estuary sees an overall decline in turbidity through time (Figure 15). This decline occurs at an approximate rate of -1.70% / year. Lawrence has an outlier in the period 1992-1995, showing a turbidity value of 298 FNU, also being the highest measured turbidity. The lowest measured turbidity occurred the period before, with 155 FNU. This differs significantly from the first and last period turbidity levels, which have 222 FNU and 166 FNU respectively.

The standard deviation of the Lawrence turbidity measurements is 43.5, with a range of 142.9 FNU. However, if the outlier of 298 FNU is excluded, the standard deviation lowers to 21.5 and the range changes to 67.3 FNU.

Change in Morphology

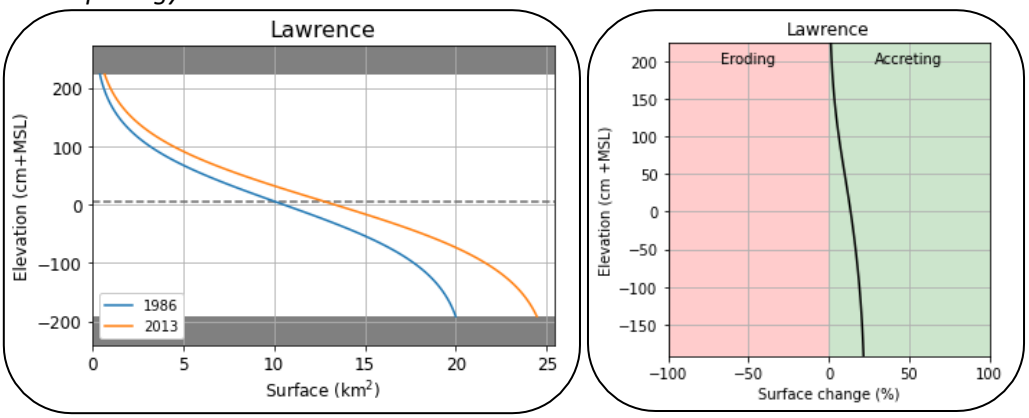

Figure 16: The hypsometric curve of Lawrence is shown on the left. The right figure shows the morphology interpretation.

Lawrence is a slightly accreting estuary at all elevations (Figure 16). The largest change relative to 1986 occurred at the lower elevation levels. Lawrence shows signs of a flattening accreting estuary.

A spearman correlation calculated over the saltmarsh area through time and the turbidity through time of Lawrence gave a value of -0.567 with a *p*-value of 0.1116. A negative correlation means a decrease in turbidity corresponds with an increase in saltmarsh area.

<u>Westerschelde</u>
Area classification

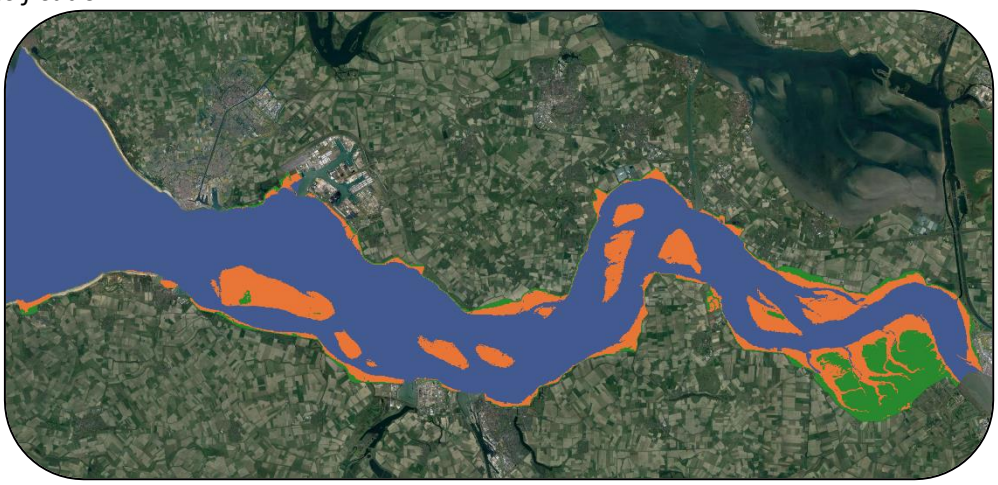

Figure 17: Westerschelde, an estuary in the province of Zeeland, The Netherlands. The different colours indicate the different land cover types as per 2013 (Green = Saltmarsh, Brown = Mudflat).

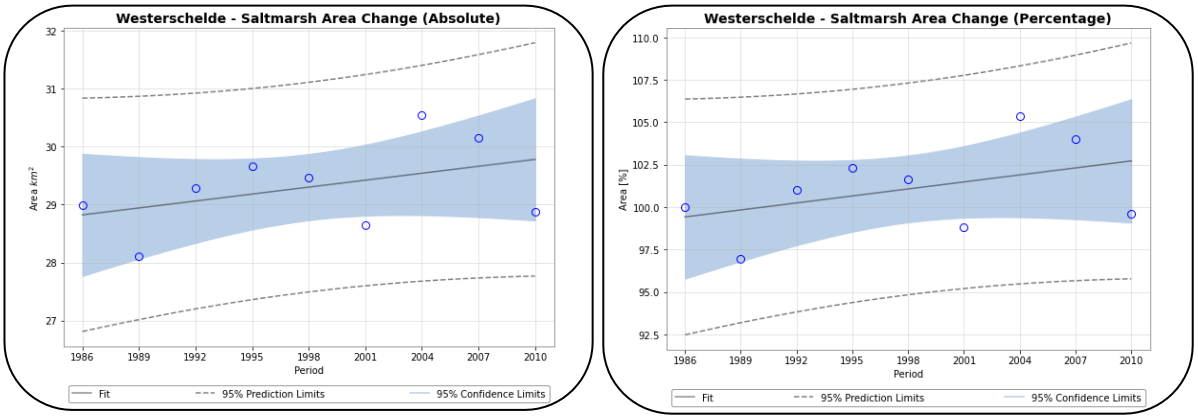

Figure 18: The left figure shows change in saltmarsh area in the Westerschelde between the periods 1986 and 2013 in absolute values. The right figure shows the percentage of saltmarsh area change of every period when compared to the first period.

Most of the saltmarsh area in the Westerschelde can be found in the eastern part, a part related to the Saeftinghe saltmarsh (Figure 17). Furthermore, this saltmarsh area is quite stable. The different between the saltmarsh area in the first period and last period is only 0.1km^2, from 29.0km^2 to 28.9km^2 (Figure 18). The mean change in saltmarsh area per year is an approximate 0.14%. The largest recorded saltmarsh area is 30.5 km^2 in the period 2004 – 2007. The period with the small saltmarsh area is 1989 – 1992 with a total saltmarsh area of 28.1 km^2.

Turbidity calculations

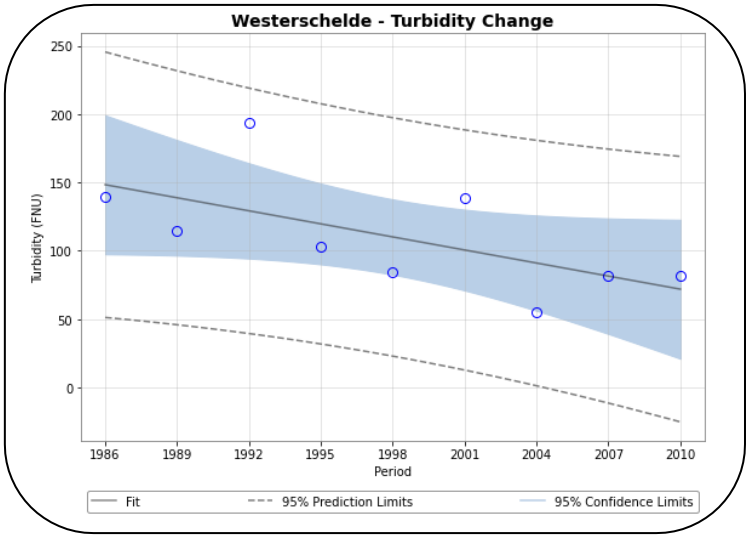

Figure 19: The change in turbidity between the periods 1986-1989 and 2010-2013 for the Westerschelde are shown in this figure.

The turbidity in the Westerschelde shows a steady decline of -3.19% per year (Figure 19). The period 1992-1995 shows itself as an outlier with the highest turbidity, with a turbidity level of 194 FNU, compared to the turbidity of the first period: 139 FNU. The lowest calculated turbidity in the Westerschelde was 54.8 FNU in the period 2004 – 2007.

The standard deviation of the Westerschelde turbidity measurements is 41.9, with a range of 138.7 FNU. However, if the outlier of 298 FNU is excluded, the standard deviation lowers to 25.9 and the range changes to 84.5 FNU.

Change in Morphology

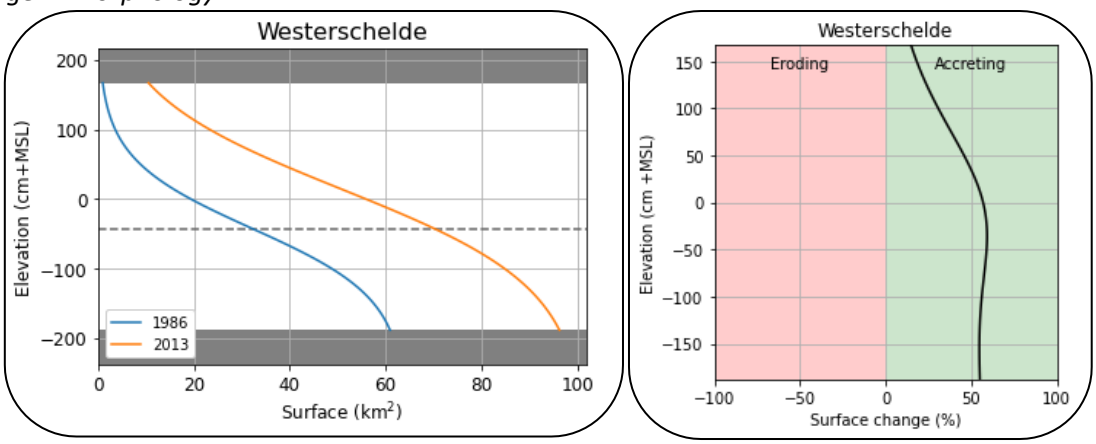

Figure 20: The hypsometric curve of the Westerschelde is shown on the left. The right figure shows the morphology interpretation by the hypsometric tool.

The Westerschelde shows a large increase in surface area when compared to the surface values of 1986 (Figure 20). The hypsometric tool shows the Westerschelde as an accreting estuary across most elevations. The largest change in elevation occurs on the lower flats.

The Simple spearman correlation for the Westerschelde saltmarsh area change and turbidity change is -0.583 (p = 0.0992). In the Westerschelde, a decrease in turbidity correlates to an increase in saltmarsh area.

<u>Mottoma</u>

Area classification

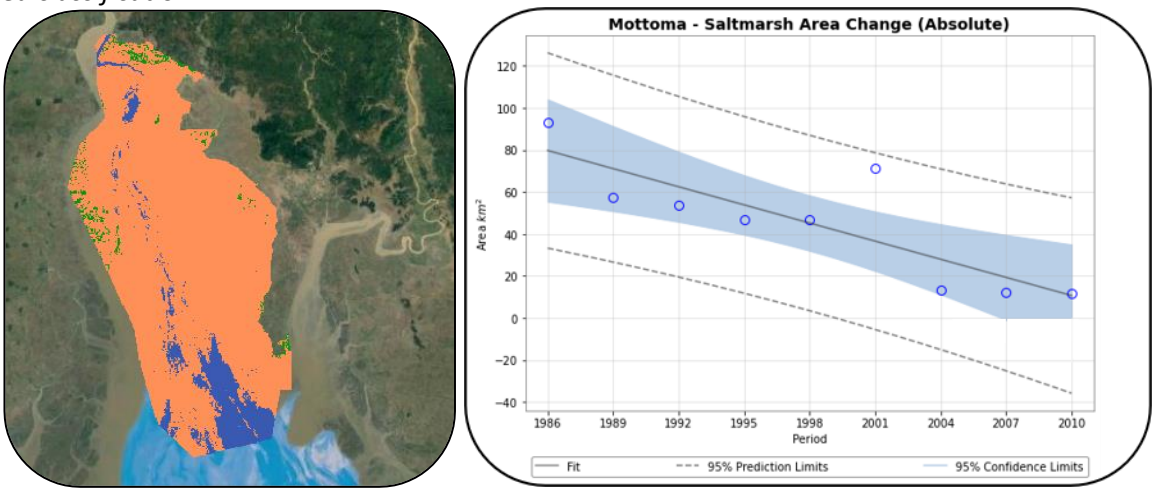

Figure 21: Mottoma is an estuary fed by the Sittaung River, in the gulf of Martaban, Myanmar. The different colours indicate the different land cover types as per 2013 (Green = Saltmarsh, Brown = Mudflat) (left image). The right figure shows change in saltmarsh area in Mottoma estuary between the periods 1986 and 2013.

The saltmarsh area of Mottoma (Figure 21) in the first period totals approximately 93.1 km^2, the highest measured saltmarsh area during the time frame of this study. In the period 2010 – 2013 this has significantly decreased to a total square km area of approximately 11.5 km^2. The saltmarsh area decline of Mottoma has a mean slope of -3.25% per year.

Turbidity calculation

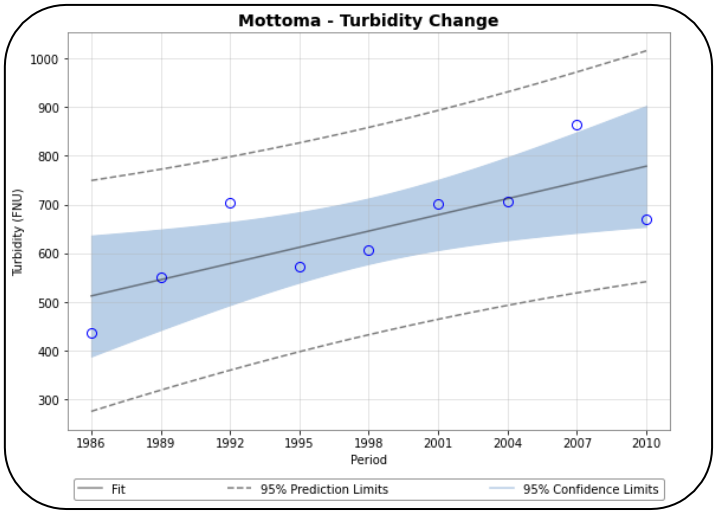

Figure 22: The change in turbidity between the periods 1986-1989 and 2010-2013 for the Mottoma estuary are shown in this figure.

Mottoma estuary sees an overall increase in turbidity through time (Figure 22). This increase occurs at an approximate rate of 1.96% / year. The highest turbidity value was calculated over the period 2007 – 2010, amounting to a total turbidity of 863 FNU. The lowest measured turbidity occurred in the first period of this study with a turbidity value of 437 FNU.

The standard deviation of the Mottoma turbidity measurements is 121.1, with a range of 426.3 FNU.

Change in Morphology

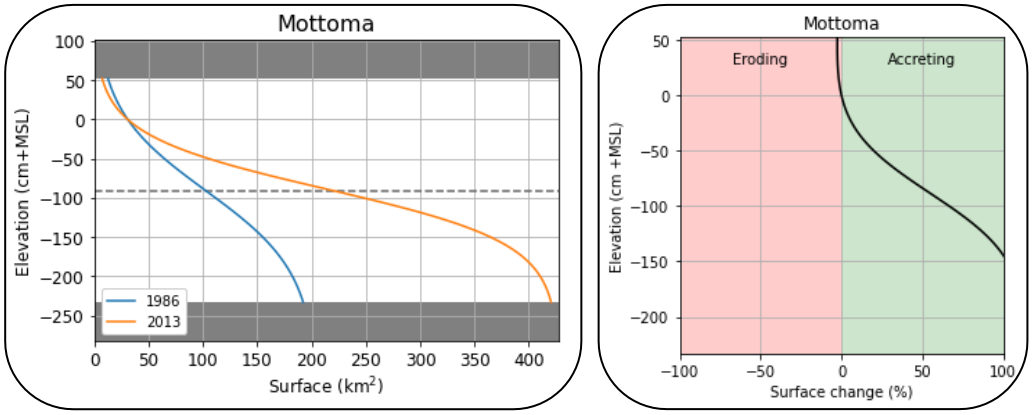

Figure 23: The hypsometric curve of Mottoma is shown on the left. The right figure shows the morphology interpretation.

Mottoma shows a large increase in surface area when compared to the surface values of 1986 (Figure 23). The hypsometric tool shows Mottoma as an especially strong accreting estuary across the lower flats. The higher elevated areas above mean sea level are stable.

The Simple spearman correlation for the Mottoma saltmarsh area change and turbidity change is -0.55 (p = 0.1250). There is no real significant correlation between a change in turbidity and a change in saltmarsh area according to the spearman correlation test in Mottoma.

Saint Michel

Area classification

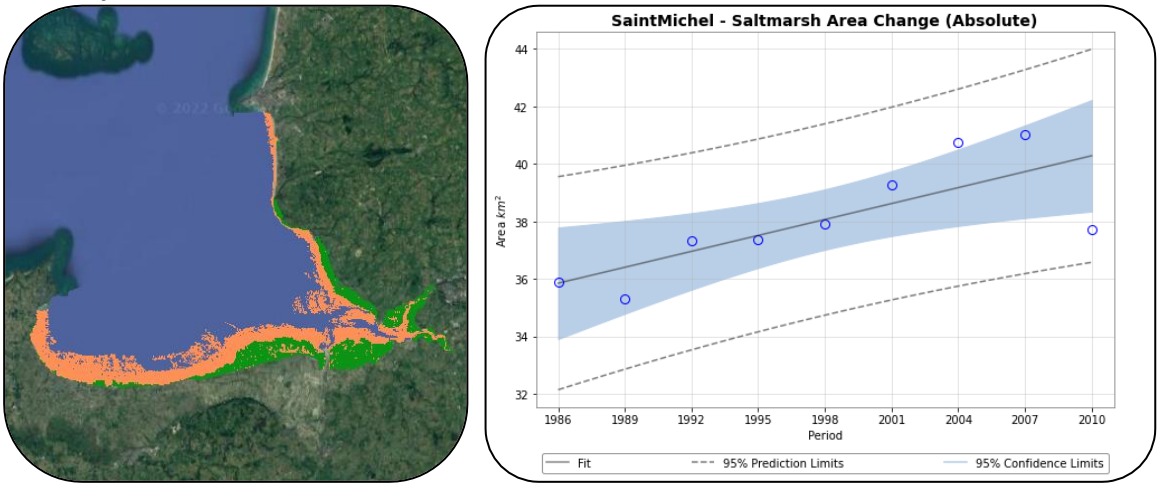

Figure 24: Saint Michel is an estuary fed by river Couesnon, in the French department Manche, in Normandy. The different colours indicate the different land cover types as per 2013 (Green = Saltmarsh, Brown = Mudflat) (left image). The right figure shows change in saltmarsh area in Lawrence estuary between the periods 1986 and 2013.

The saltmarsh area of Saint Michel (Figure 24) in the first period totals approximately 35.9 km^2. In the period 2010 – 2013 this has increased to a total square km area of approximately 37.7 km^2. The highest saltmarsh area was measured in the period 2007 – 2010, totalling 41.0 km^2, whereas the lowest measured saltmarsh area occurred in the period 1989 – 1992. The total saltmarsh area in that period was 35.3 km^2. Overall, the saltmarsh area increase of Saint Michel has a mean slope of 0.19% per year.

Turbidity calculation

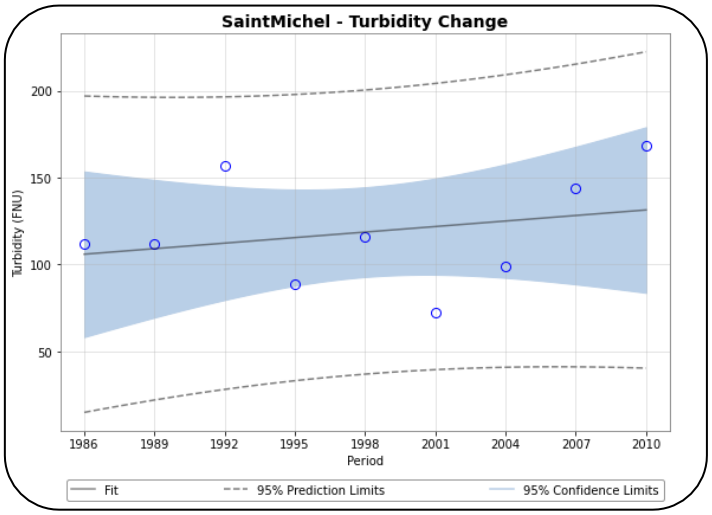

Figure 25: The change in turbidity between the periods 1986-1989 and 2010-2013 for the Saint Michel estuary are shown in this figure.

The turbidity in Saint Michel overall shows a slight increase of 1.19% per year (Figure 25). However, there are again some outliers that skew the data. The lowest recorded turbidity during the study period was 72 FNU in the period 2001 – 2004. The highest recorded turbidity occurred in the period 2010 – 2013, totalling 168 FNU. The turbidity measured at the start of the study period was 111 FNU.

The standard deviation of the Saint Michel turbidity measurements is 31.9, with a range of 96.4 FNU.

Change in Morphology

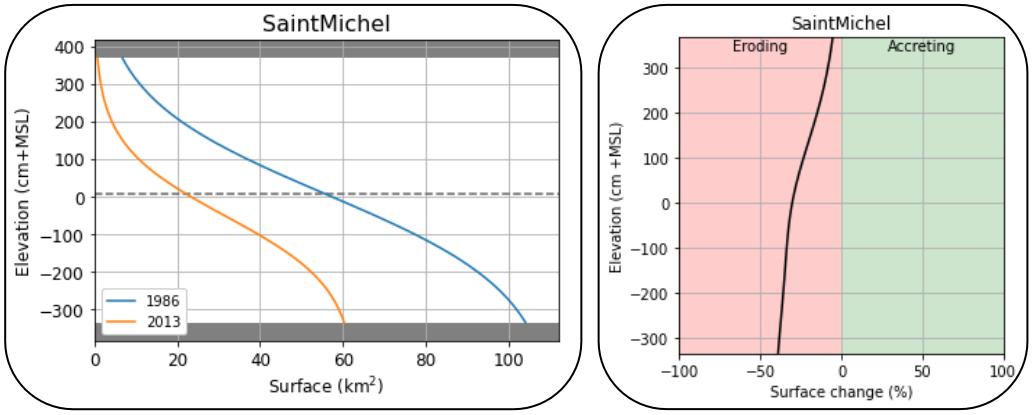

Figure 26: The hypsometric curve of the Saint Michel estuary is shown on the left. The right figure shows the morphology interpretation.

There is a steady change in surface area in Saint Michel when compared to the surface values of 1986 (Figure 26). The hypsometric tool shows Saint Michel as an eroding estuary across all elevation levels. The eroding is stronger in the lower elevation levels.

The Simple spearman correlation for the Saint Michel saltmarsh area change and turbidity change is -0.08 ($p = 0.8312$). According to the spearman correlation test there is no significant correlation between a change in turbidity and a change in saltmarsh area in Saint Michel.

Statistical justification

The index of dispersion for Arcachon, Lawrence, Westerschelde and Saint Michel are all close to 1 and show that the date collection does not introduce any significant clustering (Table 1). The index of dispersion values for the water level in Mottoma however, do deviate more from 1. This indicates the occurrence of clustering in the Mottoma image collection regarding Water Level. A visualisation of the data the index of dispersion is calculated from can be found in Appendix B1:B8. The lack of datapoints in the periods 1989-1992, 1992-1995 and 2001-2004 are contributing to this clustering (Appendix B3).

Table 1: The dispersion index for Arcachon, Lawrence and Westerschelde, Mottoma and Saint Michel. The Julian Day column gives the dispersion index for what Julian day the images were taken on. The Date column refers to the exact date each image was taken on. The water level column shows the dispersion index for the tide compared to the tidal range each image was taken on.

Arcachon	*Julian Day*	*Date*	*Water Level*
Incoming	*0.963*	*0.979*	*0.958*
Outgoing	*0.963*	*0.990*	*0.962*
Total	*0.966*	*0.986*	*0.962*

Lawrence	*Julian Day*	*Date*	*Water Level*
Incoming	*0.983*	*0.998*	*0.984*
Outgoing	*0.980*	*0.987*	*0.973*
Total	*0.984*	*0.997*	*0.988*

Mottoma	*Julian Day*	*Date*	*Water Level*
Incoming	*0.926*	*0.987*	*0.712*
Outgoing	*0.886*	*0.957*	*0.861*
Total	*0.913*	*0.987*	*0.787*

St Michel	*Julian Day*	*Date*	*Water Level*
Incoming	*0.970*	*0.989*	*0.990*
Outgoing	*0.920*	*0.930*	*0.957*
Total	*0.959*	*0.982*	*0.990*

Wester-schelde	*Julian Day*	*Date*	*Water Level*
Incoming	*0.968*	*0.990*	*0.971*
Outgoing	*0.962*	*0.996*	*0.967*
Total	*0.965*	*0.994*	*0.971*

Table 2 shows the mean number of usable images per period from all estuaries combined. Both the period 2001-2004 and 2010-2013 show a significant drop in image count when compared to the other periods. The image count per estuary per period can be found in Appendix A9.

Table 2: The mean number of images used in each per period in this study.

	1986 - 1989	*1989 - 1992*	*1992 - 1995*	*1995 - 1998*	*1998 - 2001*	*2001 - 2004*	*2004 - 2007*	*2007 - 2010*	*2010 - 2013*
Images	*33*	*38.9*	*39.4*	*42.5*	*37.5*	*23.7*	*43.7*	*35.9*	*24.6*

All data

The area calculation results for all the estuaries can be found in Appendix A1:A4**.** Out of all estuaries in this study, approximately 77.8% saw an increase in saltmarsh area between the periods 1986 and 2013. 15.6% experienced a decline in saltmarsh area and there was not sufficient data to accurately calculated a trend for 6.7% of the estuaries.

The turbidity calculation results for all estuaries can be found in Appendix A1:A4. Out of all studied estuaries, 82.2% experienced a decline in turbidity through time. 13.3% saw an increase in turbidity between 1986 and 2013 and 4.4% of the estuaries lacked sufficient data.

The results of the hypsometric tool for all estuaries in this study can be found in Appendix A5. Out of all estuaries, 42.2% were found to be eroding whereas 31.1% were accreting estuaries. 15.6% of the estuaries were relatively stable through the period 1986-2013. For 11.1% of the estuaries the data was not sufficient to determine a trend in elevation change through time.

Out of all estuaries in this study, 75.6% are considered to have high turbid waters (>23 FNU) when looking at the median values of the turbidity between 1986 and 2013. Respectively, 24.4% of the estuaries are considered to have low turbid waters. Out of the high turbid estuaries, 82.4% experienced a decline in turbidity through time, whereas an increase in turbidity was measured for 14.7%. For 2.9% of the high turbid estuaries, there was insufficient data available to determine the trend of its turbidity through time. Out of the low turbid estuaries, 90.9% of the estuaries experienced a decline in turbidity through time, 9.1% of the estuaries experienced an increase in turbidity through time. These results, including the standard deviation, range and median of the turbidity of all estuaries can be found in Appendix A6.

The correlation results for all estuaries can be found in Appendix A7**.** Out of all estuaries in this study, approximately 84.4% had a negative correlation between saltmarsh area change through time and turbidity change through time. In other words, if the correlation is significant, more often than not an increase in turbidity is correlated with a decrease in saltmarsh area. 4.4% had incorrect or insufficient data.

The correlation between the turbidity trend and the accretion or erosion based on the hypsometric curve can be found in Appendix A8 for all estuaries. 38% of all estuaries showed a positive correlation, 24% showed no clear correlation either due to an error in measurements or no real accretion or erosion being detected and again 38% of all estuaries had a negative correlation.

Discussion

To assess whether turbidity affects the morphology of estuaries and tidal flats, a correlation between these two variables is needed. However, the morphology variable in this study is made up out of elevation change and saltmarsh change. According to the Spearman correlation test results, turbidity change and elevation change was found to be both positive and negative in 38% of the estuaries, making it difficult to ascertain whether a change in turbidity has an effect on the elevation change of an estuary through time. However, 84.4% of the estuaries in this study saw a negative correlation between turbidity change through time and saltmarsh area through time, meaning more often than not a decrease in turbidity levels was accompanied by an increase in saltmarsh area. This does not prove that a change in turbidity is the cause for a change in saltmarsh area in an estuary, nor is the correlation always significant. It does however, show that turbidity can be an influence on the saltmarsh area of estuaries. A change in turbidity could potentially even be a predictor for saltmarsh change when smaller timeframes are used. These findings agree with Willemsen et al. (2022), in that sediment supply potentially has an effect on saltmarsh extent. However, according to Willemsen et al. (2022), eroding saltmarshes switched to an accreting behaviour when suddenly supplied with a surplus of sediment, which is the opposite of what was found in this study. However, the different findings may be due to the fact that sediment supply and turbidity are not the same. A decrease in turbidity does not necessarily imply a decrease in sediment supply available for saltmarshes of an estuary. A decrease in turbidity could also point towards an increase in sediment deposition, which in turn increases the sediment supply available for saltmarshes. This is in line with findings of Liu et al. (2021), whom states that coastal wetlands growth relies primarily on sediment availability as opposed to other factors such as wetland elevation, tidal range or wave action. This is due to saltmarshes trapping sediment, thereby increasing sediment deposition rates (Liu et al., 2021). This would mean that an increase in saltmarshes could actually lead to an increase in sediment deposition through sediment trapping, which in turn could decrease the turbidity of the water column.

Turbidity Calculations

If turbidity is correlated to morphological changes in estuaries and tidal flats, it is important to know the trend and subsequent factors influencing this trend. The turbidity calculations in this study suggest a general decline in turbidity in estuaries worldwide. Out of all studied estuaries, 82.2% experienced a decline in turbidity between 1986 and 2013 and only 13.3% saw an increase. However, the extent of the change in turbidity over time does differ strongly between estuaries. Mottoma for example, saw its turbidity almost double, whereas the turbidity of the Arcachon estuary remained relatively stable, with a decline of only -0.16% per year. The cause of this difference is difficult to pinpoint. For one, the waters of Mottoma estuary are classified as high turbid waters, whereas Arcachon has low turbid waters. However, whether an estuary has low or high turbid waters seems to be no strong significant indicator for the trend in turbidity over time. Out of all the estuaries, 24.4% are considered to have low turbid waters, and 76.6% high turbid waters. 82.4% out of the high turbid estuaries experienced a decline in turbidity over time and 90.9% of the low turbid estuaries experienced a negative trend in turbidity. As mentioned earlier, sediment entrapment and an increase deposition rate are a more likely contributing factor. Additional, anthropogenic effects can also play a large role in the decrease in turbidity throughout the world, since most coastal regions around the world are densely populated. According to Syvitski et al. (2005, 2009), the sediment erosion has increased due to anthropogenic impacts, but the sediment reaching the actual oceans and coasts has been drastically reduced due to dams and reservoirs. Furthermore, Li et al., (2019) found that annual water flux rates in rivers and estuaries worldwide remained stable, while sediment fluxes decrease by 20%, further strengthening the narrative that anthropogenic barriers are affecting the sediment concentration and thus the turbidity of estuaries worldwide. The overall decline of turbidity globally as seen in this study is in line with these findings.

Area Calculations

The saltmarsh area of estuaries worldwide was also found to have increased in most estuaries. This is in line with the findings of Laengner et al. (2019), who assessed the extent of saltmarshes in Europe. They found a significant increase in saltmarsh extent in 68% of the 125 estuaries in the study. However, according to Murray et al. (2019) the overall global tidal flat extent has decline by 16% between 1984 and 2016. The findings of this study and Laengner et al. (2019), and the findings of Murray et al. (2019) however do not necessarily oppose each other, since the definition of tidal flats generally include the saltmarsh and the mudflat. The results of these studies could therefore indicate a continued decline of mudflat as opposed to a decline in saltmarsh.

To assess whether the global decline of tidal flat extent is largely due to a decline in mudflat, the mudflat area change through time needs to be determined. The area classification method in this study showed that if accurate shapefiles are provided, it does not matter where the estuary is located, area classifications can be made. Therefore, the mudflat extent of all estuaries was calculated in a similar manner to which the saltmarsh area was determined. However, the mudflat area change results are not used in this study due to there being to much variation in each data point through time. There are a couple of potential reasons for these variations and why mudflat are more difficult to accurately define than saltmarsh area through this method.

First of, mudflats are the parts of a tidal flat which are most frequently inundated (figure 1). This effectively means that depending on the tide at the time an image is taken, the size of the mudflat can vary significantly. Saltmarshes are the part of the tidal flats which are the least inundated and are therefore less susceptible to large variations in size due to the tidal datum. Secondly, extreme events such as spring tides and storm surges have a larger effect on mudflats than saltmarshes. Mudflats consist of loose material such as sand and silt and are more morphodynamic than saltmarshes (Deppe, 1999; Pritchard & Hogg, 2003). Therefore, they are more likely to change morphologically by such an event (Mariotti & Fagherazzi, 2013). Saltmarshes on the other hand consist of vegetation and exist in a more morphodynamic equilibrium (Friedrichs, 2012). Therefore, they are less likely to be majorly effected by a single event (Spencer et al., 2016). If Landsat images are taken at the time of such an event, this could lead to drastic outliers regarding mudflats area. Lastly, in high turbid estuaries, parts of the water channel may be classified as mudflat instead. This can happen when the turbidity is high enough to change the reflective properties of water enough for a false classification to occur. Dogliotti et al. (2015) also warns for this to have a potential effect on the turbidity calculations, if estuaries are determined to have a turbidity 1000 FNU or higher. Due to these reasonings, the mudflat calculated area change through time is not used in this study. Potential solutions to increase the accuracy of the mudflat calculations can be found in the *Discussion – Method Assessment* section of this study.

Morphology Changes

The hypsometric tool showed that out of all estuaries, 42.2% were found to be eroding whereas 31.1% were accreting and 15.6% of the estuaries were relatively stable through the period 1986-2013. A larger percentage of estuaries were found to be either eroding or stable, rather than accreting. These results, in conjunction with the aforementioned increase of saltmarsh area through time and the findings of Murray et al., (2019) stating a decrease in global tidal flat extent, reinforce the earlier stated hypothesis that the potential cause of the decrease in global tidal flat extent is due to a decrease in mudflats as opposed to saltmarshes.

The results of the hypsometric tool can also be used in combination with the saltmarsh area change to enhance the morphological change results of a specific estuary. For example, Arcachon shows a decrease in saltmarsh area in conjunction with the hypsometric curve showing an eroding pattern in the elevation from mean sea level and below. In this case, the estuary is most likely eroding away, with parts of the mudflat disappearing as well as saltmarsh becoming more exposed to direct tidal

action and converting into mudflat. However, caution should be used when making assessments based on the hypsometric curve, since only measurements up to the Low-water boundary are considered (figure 1). However, the accuracy of these deductions can be increased by including more data from different sources, such as vegetation trends. For Arcachon, as previously mentioned, the saltmarsh vegetation *Zostera noltii* (dwarf eelgrass) has seen a rapid decline between 1989 and 2007 (Ganthy et al., 2013). These findings reinforce the assessment that the saltmarsh of the Arcachon estuary is in decline. This method can be used assess the trend of specific estuaries, if additional data is available on the specific estuary.

Statistical Justification

Data point clustering can have a significant influence on the results of both the turbidity calculations, as well as the area classifications and hypsometric curve. Overall, the index of dispersion shows the data collection to be well dispersed and generally speaking show no significant clustering. There are a few exceptions, such as the estuary Drakes. When looking at the dispersion index based on the Julian days, most images taken are clustered around the same mean water level and the summer months. This skew in the data collection in the summer months is an example of most likely a 'good weather bias'. Most images of estuaries which pass quality and cloud cover control measures are taken on days with good weather. Depending on the geographic location of an estuary, certain months such as the summer months, have less clouds and are therefore overrepresented in datasets. A bias around the same mean water level or a specific tide can also occur, which can influence both the turbidity as well as the area classifications. This could potentially occur if the revisit period, meaning the time it takes between two observations of the same location, of a satellite is (almost) equal to the tidal period. However, this is not the case for Landsat 5. Clustering of the mean water level data points can still occur randomly however, due to for example, a good weather bias coinciding with the tidal period. An example of a bias in both mean water level and Julian days can be seen in the dispersion index figure of Chwaka (Appendix B3:B4).

Looking at the average image counts found in Table 1, both the periods 2001-2004 and 2010-2013 differ significant from other periods. This can also be seen in the index of dispersion graphs (Appendix B1:B9). Although no cause of the low image counts for the period 2001-2004 has been found, the 2010-2013 period could potentially have been caused by the multiple mechanical failures Landsat 5 endured during 2012, which eventually led to its decommissioning in early 2013 (Riebeek, 2013).

The Spearman correlations test results in this study showed various degrees of correlation between turbidity changes, area changes and elevation changes. However, these p-values of these correlations showed that they were not always significant. The p-values in a spearman correlation test are dependent on the observed correlation and the sample size, meaning a very weak correlation could be considered significant if the sample size is large enough. In the case of this study, the sample size is often only 9, the number of periods the images are sorted into. Meaning the p-value has a lower chance of being significant if a weak correlation is found. This means that the correlations given by the spearman test could potentially be caused by chance. However, the p-value gives the probability of seeing the perceived correlation, if no correlation exists. It does not necessarily mean the correlation is not present. Therefore, the correlations are only used to give indication towards a general trend.

Conceptual

Even though the actual data is not always robust enough to draw strong conclusion out of, there are still some indicators which point towards a correlation. One such concept points towards the theory of dynamic equilibrium, which states that changes in long-term trends of estuaries do not occur gradually. Rather changes occur rapidly once a steady-state threshold is breached and a new dynamic equilibrium is formed. Looking at the Mottoma saltmarsh area results, this can potentially be seen in

figure 21. A rapid change potentially occurred in 2001 – 2004 and a new steady-state is formed from 2004 onwards. However, this theory is hard to accurately depict, especially when outliers could cloud the rapid transition phases. However, this concept is in line with findings of Hu et al. (2015), who tested the dynamic equilibrium theory based spatiotemporal bed shear stress variations in tidal flats.

Method Assessment

This is the first time a uniform method was used to calculated the change in turbidity, change in saltmarsh and change in morphology on a global scale. Therefore, an assessment on the methods used could potentially provide improvements for further studies.

The data correction methods as described in the method – *data correction* (page 10), filtered out all low-quality and cloud covered images. In most cases, there were enough images of an estuary left to ensure a decent accuracy during calculations. However, for some estuaries such as Cuna and Kaipara, the number of remaining images was too low (Appendix A9). This resulted in a lower effectiveness of the mean function in reducing outliers or even no data for certain periods. This can be seen when looking at the turbidity calculations of Chwaka, where an outlier in the period 1998-2001 has approximately 4x the turbidity when compared to the first period (Appendix A2). To overcome this, either the quality control or cloud cover threshold needs to be tweaked, to allow for more images to be added to the image collection. This in turn however, does decrease the accuracy in all the following calculations. There are also known methods to overcome cloud cover by using reference images of the same area, using data from different dates (Martinuzzi et al., 2007). This method however, cannot be applied to this study because it would introduce double or false data during turbidity calculations. A longer timeframe would also diminish the effects of missing periods on trends. Therefore, the use of multiple Landsat datasets could potentially increase the overall accuracy of trends. However, as previously mentioned, there are slight differences between different Landsat satellites, which would in turn introduce a skew in the data. If this skew can be accounted for correctly, the potential for this study to more accurately determine trends could increase.

The area classification method in this study performed well for saltmarsh area, as long as accurate shapefiles were provided. For mudflat area classification however, a few aforementioned issues arose concerning the accuracy of the mudflat area classification. Although the periodically inundated nature of mudflats will always make it difficult to find the true size said mudflat and the global scale of this study makes it difficult to adjust the method to increase accuracy on a specific part of tidal flats, there are ways in which the accuracy of mudflat classification could be improved. The accuracy of the mudflat classification could be increased by correcting for the tidal datum at which each image is taken and calculating high-water boundaries and low-water boundaries for each estuary. The high-water boundary and low-water boundary are calculated by respectively taking the minimum of the maximum water level measured for each period and the maximum of the minimum water level measured for each period. These two values represent the boundaries of 'ordinary' high and low water. By not taking into account every image taken at a tidal datum above or below these values, a more accurate mudflat variation is assured. This method could reduce the effect of spring tide and storm surges on the mudflat area classification. An example of a water boundaries figure can be found in Appendix B11**.** However, there are considerations to be made if this method were to be applied. First, this method cherry-picks data. Therefore it could result in data which is more workable, but less reflective of the real-world situation. Secondly, with continued sea level rise due to climate change, the 'ordinary' high tide and low tide water levels are changing. This is especially important to consider during studies over long time periods.

The turbidity calculation method overall performed well, considering the global scale of this study. However, because the sample size is just nine periods, large outliers can have a pivoting effect on the general trend analysis of turbidity change. This should be taken into consideration before a trend

analysis is made. All in all the methodology provides a good framework for future global studies on estuaries and tidal flats.

General improvements
During the writing of this report, the Landsat 5 Surface Reflectance Tier 1 dataset has been superseded by a new dataset called the Landsat 5 Level 2, Collection 2 Tier 1. The new dataset includes a cloud quality assessment and masking tool. Therefore, the new dataset might increase the number of high-quality images in the period 2001-2004. This new dataset may also reduce the errors found in the period 1992-1995.

Another general improvement which might increase the accuracy of this study regards the creation of the shapefiles. The shapefiles used in this study were either acquired from databases or created in QGIS using Google Earth imagery. However, this imagery was not taken in the same year as the first year of Landsat 5 images used (1986). Therefore, the size of the saltmarsh of estuaries can potentially have changed beyond the borders of the shapefile.

Conclusion
This study shows that the turbidity in most tidal flats in the world is on the decline, while the saltmarsh area of these flats is increasing. Furthermore, almost half of the world's tidal flats in estuaries are eroding. In 84% of the researched tidal flats, a negative correlation was found between turbidity change and saltmarsh change, while no clear correlation was present between turbidity change and elevation change. However, the correlation between turbidity and saltmarsh extent shows that there is a link between a change in turbidity and a change in morphology in tidal flats and estuaries. A decline in turbidity seems to have positive effect on the saltmarsh area, although a direct link between the turbidity and morphology is difficult to pinpoint.

This study shows that the turbidity in most tidal flats in the world is on the decline, while the saltmarsh area of these flats is increasing. Furthermore, almost half of the world's tidal flats in estuaries are eroding. In 84% of the researched tidal flats, a negative correlation was found between turbidity change and saltmarsh change, while no clear correlation was present between turbidity change and elevation change. However, the correlation between turbidity and salt marsh extent indicates at least part of the morphology of a tidal flat in an estuary is influenced by a change in turbidity. Although a direct link between turbidity and morphology is not found, this study could provide a good framework for future research on this topic. With improvements to the method, a clearer correlation between turbidity change and morphology change could be found and help better understand the relationship between the two variables.

References

Bishop-Taylor, R., Sagar, S., Lymburner, L., Alam, I., & Sixsmith, J. (2019). Sub-Pixel Waterline Extraction: Characterising Accuracy and Sensitivity to Indices and Spectra. *Remote Sensing 2019, Vol. 11, Page 2984*, *11*(24), 2984. https://doi.org/10.3390/RS11242984

Bright, C. E., Mager, S. M., & Horton, S. L. (2018). Predicting suspended sediment concentration from nephelometric turbidity in organic-rich waters. *River Research and Applications*, *34*(7), 640–648. https://doi.org/10.1002/RRA.3305

Castelle, B., Guillot, B., Marieu, V., Chaumillon, E., Hanquiez, V., Bujan, S., & Poppeschi, C. (2018). Spatial and temporal patterns of shoreline change of a 280-km high-energy disrupted sandy coast from 1950 to 2014: SW France. *Estuarine, Coastal and Shelf Science*, *200*, 212–223. https://doi.org/10.1016/J.ECSS.2017.11.005

Costanza, R., d'Arge, R., de Groot, R., Farber, S., Grasso, M., Hannon, B., Limburg, K., Naeem, S., O'Neill, R. V., Paruelo, J., Raskin, R. G., Sutton, P., & van den Belt, M. (1997). The value of the world's ecosystem services and natural capital. *Nature 1997 387:6630*, *387*(6630), 253–260. https://doi.org/10.1038/387253A0

Dam, G., Van Der Wegen, M., Labeur, R. J., & Roelvink, D. (2016). Modelling centuries of estuarine morphodynamics in the Western Scheldt estuary. *Geophysical Research Letters*, *43*(8), 3839–3847. https://doi.org/10.1002/2015GL066725

Deppe, F. (1999). Intertidal Mudflats Worldwide. *Practical course at the Common Wadden Sea Secretariat (CWSS) in Wilhelmshaven 1st June–30th September, 36-40*.

Dogliotti, A. I., Ruddick, K. G., Nechad, B., Doxaran, D., & Knaeps, E. (2015). A single algorithm to retrieve turbidity from remotely-sensed data in all coastal and estuarine waters. *Remote Sensing of Environment*, *156*, 157–168. https://doi.org/10.1016/j.rse.2014.09.020

Dogliotti, A. I., Ruddick, K., Nechad, B., Lasta, C., Mercado, A., Hozbor, C., ... & Abelando, M. (2011). Calibration and validation of an algorithm for remote sensing of turbidity over La Plata River estuary, Argentina. EARSeL eProceedings, 10(2), 119-130.

Dronkers, J. (1986). Tidal Asymmetry and Estuarine Morphology. *Netherlands Journal of Sea Research*, *20*(3), 117–131.

Earth Engine, G. (n.d.). USGS Landsat 5 Surface Reflectance Tier 1 | *Earth Engine Data Catalog*. Retrieved August 18, 2021, from https://developers.google.com/earth-engine/datasets/catalog/LANDSAT_LT05_C01_T1_SR#bands

Fonsecal, M. S., & Fisher, J. S. (1986). A comparison of canopy friction and sediment movement between four species of seagrass with reference to their ecology and restoration. *Marine Ecology Progress Series, 29(1), 5-22*.

Friedrichs, C. T. (2012). Tidal Flat Morphodynamics: A Synthesis. *Treatise on Estuarine and Coastal Science* (Vol. 3, pp. 137–170). Elsevier Inc. https://doi.org/10.1016/B978-0-12-374711-2.00307-7

Ganthy, F., Sottolichio, A., & Verney, R. (2013). Seasonal modification of tidal flat sediment dynamics by seagrass meadows of Zostera noltii (Bassin d'Arcachon, France). *Journal of Marine Systems*, *109–110*(SUPPL.), S233–S240. https://doi.org/10.1016/J.JMARSYS.2011.11.027

Gao, S. (2018). Geomorphology and sedimentology of tidal flats. *Coastal Wetlands: An Integrated Ecosystem Approach*, 359–381. https://doi.org/10.1016/B978-0-444-63893-9.00010-1

Gippel, C. J. (1995). Potential of turbidity monitoring for measuring the transport of suspended solids in streams. *Hydrological Processes*, *9*(1), 83–97. https://doi.org/10.1002/HYP.3360090108

Google Earth Engine. (n.d.). *Earth Engine Data Catalog*. Retrieved September 5, 2021, from https://developers.google.com/earth-engine/datasets

Gullström, M., Lundén, B., Bodin, M., Kangwe, J., Öhman, M. C., Mtolera, M. S. P., & Björk, M. (2006). Assessment of changes in the seagrass-dominated submerged vegetation of tropical Chwaka Bay (Zanzibar) using satellite remote sensing. *Estuarine, Coastal and Shelf Science*, *67*(3), 399–408. https://doi.org/10.1016/J.ECSS.2005.11.020

Halper, F. B., & McGrail, D. W. (1988). Long-term measurements of near-bottom currents and suspended sediment concentration on the outer Texas-Louisiana continental shelf. *Continental Shelf Research*, *8*(1), 23–36. https://doi.org/10.1016/0278-4343(88)90022-2

Healy, T., Wang, Y., & Healy, J. (2002). Muddy Coasts of the World: Processes, Deposits, and Function. *Elsevier Science*.

Hibma, A., Stive, M. J. F., & Wang, Z. B. (2004). Estuarine morphodynamics*. Coastal Engineering, 51(8-9), 765-778.*

Hu, Z., Wang, Z. B., Zitman, T. J., Stive, M. J. F., & Bouma, T. J. (2015). Predicting long-term and short-term tidal flat morphodynamics using a dynamic equilibrium theory. *Journal of Geophysical Research: Earth Surface*, *120*(9), 1803–1823. https://doi.org/10.1002/2015JF003486

Jaewon;, W. J.-S. Y.-K. (2005). Test Application of KOMPSAT-2 to the Detection of Microphytobenthos in Tidal Flats. *Proceedings of the KSRS Conference*, 249–252.

Kalele, A. S. (2019). Estimation and mapping of turbidity in the lower Charles River Using Landsat 8 OLI satellite imagery. *A Thesis Presented, Northeastern University*.

Kirby, R. (2000). Practical implications of tidal flat shape. *Continental Shelf Research*, *20*(10–11), 1061–1077. https://doi.org/10.1016/S0278-4343(00)00012-1

Kitchener, B. G., Wainwright, J., & Parsons, A. J. (2017). A review of the principles of turbidity measurement*. Progress in Physical Geography*, 41(5), 620-642. https://doi.org/10.1177/0309133317726540

Klein, R. D., Lewis, J., & Buffleben, M. S. (2011). Logging and turbidity in the coastal watersheds of northern California. *Geomorphology.* https://doi.org/10.1016/j.geomorph.2011.10.011

Koopmans, B. N., & Wang, Y. (1994). Satellite radar data for topographic mapping of the tidal flats in the Wadden Sea, The Netherlands. *Proceedings Second Thematic Conference on Remote Sensing for Marine and Coastal Environments*.

Laengner, M. L., Siteur, K., & van der Wal, D. (2019). Trends in the Seaward Extent of Saltmarshes across Europe from Long-Term Satellite Data. *Remote Sensing*, *11*(14), 1653. https://doi.org/10.3390/rs11141653

Lee, Y., Ryu, J., & Won, J. (2005). Detection of Microphytobenthos in the Saemangeum Tidal Flat by Linear Spectral Unmixing Method. *Korean Journal of Remote Sensing*, *21*(5), 405–415.

Li, L., Ni, J., Chang, F., Yue, Y., Frolova, N., Magritsky, D., Borthwick, A. G. L., Ciais, P., Wang, Y., Zheng, C., & Walling, D. E. (2019). Global trends in water and sediment fluxes of the world's large rivers. *Science Bulletin, 65(1), 62-69.* https://doi.org/10.1016/j.scib.2019.09.012

Liu, Z., Fagherazzi, S., & Cui, B. (2021). Success of coastal wetlands restoration is driven by sediment availability. *Communications Earth & Environment 2021 2:1*, *2*(1), 1–9. https://doi.org/10.1038/S43247-021-00117-7

Mariotti, G., & Fagherazzi, S. (2013). Wind waves on a mudflat: The influence of fetch and depth on bed shear stresses. *Continental Shelf Research*, *60*, S99–S110. https://doi.org/10.1016/J.CSR.2012.03.001

Martinuzzi, S., Gould, W. A., & Gonzalez, O. M. R. (2007). Creating cloud-free Landsat ETM+ data sets in tropical landscapes: cloud and cloud-shadow removal. *U.S. Department of Agriculture, Forest Service, International Institute of Tropical Forestry. Gen. Tech. Rep. IITF-32.*, *32*. https://doi.org/10.2737/IITF-GTR-32

Merkens, J. L., Reimann, L., Hinkel, J., & Vafeidis, A. T. (2016). Gridded population projections for the coastal zone under the Shared Socioeconomic Pathways. *Global and Planetary Change*, *145*, 57–66. https://doi.org/10.1016/j.gloplacha.2016.08.009

Möller, I., Kudella, M., Rupprecht, F., Spencer, T., Paul, M., Van Wesenbeeck, B. K., Wolters, G., Jensen, K., Bouma, T. J., Miranda-Lange, M., & Schimmels, S. (2014). Wave attenuation over coastal salt marshes under storm surge conditions. *Nature Geoscience 2014 7:10*, *7*(10), 727–731. https://doi.org/10.1038/NGEO2251

Murray, N. J., Phinn, S. R., DeWitt, M., Ferrari, R., Johnston, R., Lyons, M. B., Clinton, N., Thau, D., & Fuller, R. A. (2019). The global distribution and trajectory of tidal flats. *Nature*, *565*(7738), 222–225. https://doi.org/10.1038/s41586-018-0805-8

Myre, E., Shaw, R., & Candidates, M. S. (2006). The Turbidity Tube: Simple and Accurate Measurement of Turbidity in the Field. *Michigan Technological University, 15*

Natura2000. (n.d.). *Natura 2000 End 2021 - Shapefile — European Environment Agency*. Retrieved July 11, 2022, from https://www.eea.europa.eu/data-and-maps/data/natura-13/natura-2000-spatial-data/natura-2000-shapefile-1

Nechad, B., Ruddick, K. G., & Park, Y. (2010). Calibration and validation of a generic multisensor algorithm for mapping of total suspended matter in turbid waters. *Remote Sensing of Environment*, *114*(4), 854–866. https://doi.org/10.1016/j.rse.2009.11.022

Neumann, B., Vafeidis, A. T., Zimmermann, J., & Nicholls, R. J. (2015). Future Coastal Population Growth and Exposure to Sea-Level Rise and Coastal Flooding - A Global Assessment. *PLOS ONE*, *10*(3), e0118571. https://doi.org/10.1371/journal.pone.0118571

Passeri, D. L., Hagen, S. C., Medeiros, S. C., Bilskie, M. V., Alizad, K., & Wang, D. (2015). The dynamic effects of sea level rise on low-gradient coastal landscapes: A review. In *Earth's Future* (Vol. 3, Issue 6, pp. 159–181). John Wiley and Sons Inc. https://doi.org/10.1002/2015EF000298

Pritchard, D., & Hogg, A. J. (2003). Cross-shore sediment transport and the equilibrium morphology of mudflats under tidal currents. *Journal of Geophysical Research: Oceans*, *108*(C10), 3313. https://doi.org/10.1029/2002JC001570

Riebeek, H. (2013). Historic Landsat 5 Mission Ends | *Landsat Science*. https://landsat.gsfc.nasa.gov/article/historic-landsat-5-mission-ends/

Robins, P. E., & Davies, A. G. (2010). Morphological controls in sandy estuaries: The influence of tidal flats and bathymetry on sediment transport. *Ocean Dynamics*, *60*(3), 503–517. https://doi.org/10.1007/S10236-010-0268-4/FIGURES/11

Rudorff, N., Rudorff, C. M., Kampel, M., & Ortiz, G. (2018). Remote sensing monitoring of the impact of a major mining wastewater disaster on the turbidity of the Doce River plume off the eastern Brazilian coast. *ISPRS Journal of Photogrammetry and Remote Sensing*, *145*, 349–361. https://doi.org/10.1016/J.ISPRSJPRS.2018.02.013

Spencer, T., Möller, I., Rupprecht, F., Bouma, T. J., Wesenbeeck, B. K. van, Kudella, M., Paul, M., Jensen, K., Wolters, G., Miranda-Lange, M., & Schimmels, S. (2016). Salt marsh surface survives true-to-scale simulated storm surges. *Earth Surface Processes and Landforms*, *41*(4), 543–552. https://doi.org/10.1002/ESP.3867

Sun, C., Liu, Y., Zhao, S., Zhou, M., Yang, Y., & Li, F. (2016). Classification mapping and species identification of salt marshes based on a short-time interval NDVI time-series from HJ-1 optical imagery. *International Journal of Applied Earth Observation and Geoinformation*, *45*, 27–41. https://doi.org/10.1016/J.JAG.2015.10.008

Syvitski, J. P. M., Kettner, A. J., Overeem, I., Hutton, E. W. H., Hannon, M. T., Brakenridge, G. R., Day, J., Vörösmarty, C., Saito, Y., Giosan, L., & Nicholls, R. J. (2009). Sinking deltas due to human activities. *Nature Geoscience*, *2*(10), 681–686. https://doi.org/10.1038/ngeo629

Syvitski, J. P. M., Vörösmarty, C. J., Kettner, A. J., & Green, P. (2005). Impact of humans on the flux of terrestrial sediment to the global coastal ocean. *Science*, *308*(5720), 376–380. https://doi.org/10.1126/SCIENCE.1109454/SUPPL_FILE/SYVITSKI.SOM.PDF

Szabó, S., Gácsi, Z., & Boglárka, B. (2016). Specific features of NDVI, NDWI and MNDWI as reflected in land cover categories. *Landscape & Environment*, *10*(3–4), 194–202. https://doi.org/10.21120/LE/10/3-4/13

The World's Protected Areas. (n.d.). *ProtectedPlanet*. Retrieved September 4, 2021, from https://www.protectedplanet.net/en

Tong, S. S., Deroin, J. P., & Pham, T. L. (2020). An optimal waterline approach for studying tidal flat morphological changes using remote sensing data: A case of the northern coast of Vietnam. *Estuarine, Coastal and Shelf Science*, *236*, 106613. https://doi.org/10.1016/J.ECSS.2020.106613

United Nations. (2017). The Ocean Conference: People and Oceans. *The United Nations.*

USGS. (n.d.-a). Landsat 5 | *U.S. Geological Survey*. Retrieved July 11, 2022, from https://www.usgs.gov/landsat-missions/landsat-5

USGS. (n.d.-b). Landsat Collection Quality Assessment Bands | *U.S. Geological Survey*. Retrieved July 11, 2022, from https://www.usgs.gov/landsat-missions/landsat-collection-2-quality-assessment-bands

USGS. (n.d.-c). Turbidity and Water. *USGS*. Retrieved September 4, 2021, from https://www.usgs.gov/special-topic/water-science-school/science/turbidity-and-water?qt-science_center_objects=0#qt-science_center_objects

van der Wal, D., Wielemaker-Van den Dool, A., & Herman, P. M. J. (2008). Spatial patterns, rates and mechanisms of saltmarsh cycles (Westerschelde, The Netherlands). *Estuarine, Coastal and Shelf Science*, *76*(2), 357–368. https://doi.org/10.1016/J.ECSS.2007.07.017

van der Wal, D., Wielemaker-van den Dool, A., & Herman, P. M. J. (2010). Spatial Synchrony in Intertidal Benthic Algal Biomass in Temperate Coastal and Estuarine Ecosystems. *Ecosystems 2010 13:2*, *13*(2), 338–351. https://doi.org/10.1007/S10021-010-9322-9

Van Der Wegen, M., & Roelvink, J. A. (2008). Long-term morphodynamic evolution of a tidal embayment using a two-dimensional, process-based model. *Journal of Geophysical Research: Oceans*, *113*(C3), 3016. https://doi.org/10.1029/2006JC003983

van der Wegen, M., Wang, Z. B., Savenije, H. H. G., & Roelvink, J. A. (2008). Long-term morphodynamic evolution and energy dissipation in a coastal plain, tidal embayment. *Journal of Geophysical Research: Earth Surface*, *113*(F3), 3001. https://doi.org/10.1029/2007JF000898

van Maldegem, D. C., & van Pagee, J. A. (2005). Zandhonger Oosterschelde. *Rijksinstituut voor Kust en Zee.*

Verduin, J. J., & Backhaus, J. O. (2000). Dynamics of Plant–Flow Interactions for the Seagrass Amphibolis antarctica: Field Observations and Model Simulations. *Estuarine, Coastal and Shelf Science*, *50*(2), 185–204. https://doi.org/10.1006/ECSS.1999.0567

Weiffen, M., Möller, B., Mauck, B., & Dehnhardt, G. (2006). Effect of water turbidity on the visual acuity of harbor seals (Phoca vitulina). *Vision Research*, *46*(11), 1777–1783. https://doi.org/10.1016/J.VISRES.2005.08.015

Willemsen, P. W. J. M., Smits, B. P., Borsje, B. W., Herman, P. M. J., Dijkstra, J. T., Bouma, T. J., & Hulscher, S. J. M. H. (2022). Modeling Decadal Salt Marsh Development: Variability of the Salt Marsh Edge Under Influence of Waves and Sediment Availability. *Water Resources Research*, *58*(1), e2020WR028962. https://doi.org/10.1029/2020WR028962

Won, J. S., Lee, Y. K., & Choi, J. (2005). Application of KOMPSAT-2 to the detection of microphytobenthos in tidal flats. *International Geoscience and Remote Sensing Symposium (IGARSS)*, *1*, 437–440. https://doi.org/10.1109/IGARSS.2005.1526204

Worldtides. (n.d.). WorldTides - Tide predictions for any location in the world. Retrieved September 5, 2021, from https://www.worldtides.info/

Wu, Q. (2020). geemap: A Python package for interactive mapping with Google Earth Engine. *Journal of Open Source Software*. https://doi.org/10.21105/JOSS.02305

Yang, S. L., Milliman, J. D., Li, P., & Xu, K. (2011). 50,000 dams later: Erosion of the Yangtze River and its delta. *Global and Planetary Change*, *75*(1–2), 14–20. https://doi.org/10.1016/j.gloplacha.2010.09.006

Young, N. E., Anderson, R. S., Chignell, S. M., Vorster, A. G., Lawrence, R., & Evangelista, P. H. (2017). A survival guide to Landsat preprocessing. *Ecology*, *98*(4), 920–932. https://doi.org/10.1002/ECY.1730

Ziegler, A. (2002). Issues Related to use of Turbidity Measurements as a Surrogate for Suspended Sediment. *Turbidity and Other Sediment Surrogates Workshop*, *2*, 0–3.

Appendix A

Area calculation and Turbidity calculation

Period	Estuary	Turbidity	Mudflat	Saltmarsh
1986-1989	Westerschelde	139.343	80.802	28.992
1989-1992	Westerschelde	115.069	94.004	28.104
1992-1995	Westerschelde	193.513	98.663	29.292
1995-1998	Westerschelde	103.025	92.760	29.655
1998-2001	Westerschelde	84.157	90.650	29.461
2001-2004	Westerschelde	138.601	95.709	28.641
2004-2007	Westerschelde	54.844	99.471	30.542
2007-2010	Westerschelde	81.475	97.393	30.150
2010-2013	Westerschelde	81.644	98.124	28.883
1986-1989	Oosterschelde	46.488	65.258	9.136
1989-1992	Oosterschelde	26.838	93.902	9.447
1992-1995	Oosterschelde	59.638	103.282	9.412
1995-1998	Oosterschelde	22.406	104.696	10.003
1998-2001	Oosterschelde	14.307	97.015	10.267
2001-2004	Oosterschelde	32.987	95.800	10.222
2004-2007	Oosterschelde	12.649	90.330	11.572
2007-2010	Oosterschelde	14.404	87.204	10.225
2010-2013	Oosterschelde	12.724	94.413	9.336
1986-1989	Arcachon	16.072	87.853	28.322
1989-1992	Arcachon	19.032	89.855	45.452
1992-1995	Arcachon	28.528	94.332	25.841
1995-1998	Arcachon	14.012	99.172	35.625
1998-2001	Arcachon	12.443	106.445	40.021
2001-2004	Arcachon	14.014	96.194	32.321
2004-2007	Arcachon	21.397	96.208	19.929
2007-2010	Arcachon	16.037	101.485	18.216
2010-2013	Arcachon	14.624	87.889	14.098
1986-1989	Blackwater	119.725	38.795	16.116
1989-1992	Blackwater	137.525	40.864	15.587
1992-1995	Blackwater	271.967	41.078	16.773
1995-1998	Blackwater	92.273	35.740	14.908
1998-2001	Blackwater	80.265	36.386	15.929
2001-2004	Blackwater	69.029	34.872	15.755
2004-2007	Blackwater	87.793	36.006	16.982
2007-2010	Blackwater	40.147	37.573	16.876
2010-2013	Blackwater	88.936	37.820	17.452
1986-1989	Colne	143.502	24.914	14.533
1989-1992	Colne	172.866	25.582	14.034
1992-1995	Colne	311.403	25.301	13.845
1995-1998	Colne	174.089	22.777	13.708
1998-2001	Colne	158.894	22.777	14.303
2001-2004	Colne	152.419	21.747	14.155
2004-2007	Colne	170.688	22.171	14.520
2007-2010	Colne	195.224	22.826	13.999
2010-2013	Colne	172.798	24.378	14.336
1986-1989	Humber	213.166	192.069	15.208
1989-1992	Humber	217.845	143.641	21.512
1992-1995	Humber	299.448	230.575	19.449
1995-1998	Humber	210.598	206.971	22.250
1998-2001	Humber	196.569	210.385	23.166
2001-2004	Humber	162.809	197.605	24.160
2004-2007	Humber	215.160	202.683	25.588
2007-2010	Humber	173.412	180.609	25.057
2010-2013	Humber	179.332	211.605	27.677

Period	Estuary	Turbidity	Mudflat	Saltmarsh
1986-1989	Eden	16.772	57.685	5.264
1989-1992	Eden	13.777	47.801	5.620
1992-1995	Eden	63.818	98.523	5.238
1995-1998	Eden	18.281	55.421	5.606
1998-2001	Eden	24.735	61.613	4.935
2001-2004	Eden	18.341	68.735	7.515
2004-2007	Eden	16.487	64.260	4.765
2007-2010	Eden	17.630	65.104	5.267
2010-2013	Eden	13.556	49.244	5.761
1986-1989	Olhao	68.628	53.127	7.087
1989-1992	Olhao	16.344	49.815	5.162
1992-1995	Olhao	77.522	54.135	7.184
1995-1998	Olhao	42.032	54.756	15.105
1998-2001	Olhao	32.572	54.991	18.380
2001-2004	Olhao	52.095	55.403	11.354
2004-2007	Olhao	60.742	52.603	11.087
2007-2010	Olhao	52.971	56.454	20.485
2010-2013	Olhao	64.852	50.645	15.216
1986-1989	Exe	131.848	7.900	1.339
1989-1992	Exe	45.962	8.067	1.360
1992-1995	Exe	137.508	10.866	1.404
1995-1998	Exe	45.362	11.222	1.461
1998-2001	Exe	58.795	9.208	1.366
2001-2004	Exe	142.051	9.859	1.543
2004-2007	Exe	17.306	10.606	1.478
2007-2010	Exe	51.871	11.271	1.599
2010-2013	Exe	55.323	9.431	1.468
1986-1989	Plymouth	43.931	13.587	3.156
1989-1992	Plymouth	22.629	13.707	3.231
1992-1995	Plymouth	10.051	16.575	3.199
1995-1998	Plymouth	1.681	13.523	3.231
1998-2001	Plymouth	21.319	13.333	3.155
2001-2004	Plymouth	22.766	14.755	3.487
2004-2007	Plymouth	12.853	15.076	3.420
2007-2010	Plymouth	12.417	14.182	3.499
2010-2013	Plymouth	11.628	15.944	3.596
1986-1989	SaintMichel	111.721	137.904	35.883
1989-1992	SaintMichel	111.731	111.645	35.324
1992-1995	SaintMichel	156.692	132.085	37.321
1995-1998	SaintMichel	88.695	120.375	37.361
1998-2001	SaintMichel	116.001	122.472	37.929
2001-2004	SaintMichel	72.088	139.654	39.287
2004-2007	SaintMichel	98.703	151.963	40.765
2007-2010	SaintMichel	143.870	127.939	41.009
2010-2013	SaintMichel	168.482	111.372	37.728
1986-1989	Medway	108.483	42.694	15.397
1989-1992	Medway	153.529	42.813	14.763
1992-1995	Medway	265.483	44.306	14.895
1995-1998	Medway	95.392	38.123	14.967
1998-2001	Medway	102.066	42.615	14.956
2001-2004	Medway	77.232	39.471	15.815
2004-2007	Medway	99.880	40.857	14.938
2007-2010	Medway	103.410	43.125	14.616
2010-2013	Medway	77.122	43.504	15.246

Figure A1: The first part of the results of the turbidity and area calculations. This part includes the calculations from Westerschelde to Medway. The unit of the mudflat and saltmarsh values are km^2.

Period	Estuary	Turbidity	Mudflat	Saltmarsh
1986-1989	Authie	201.486	11.505	3.319
1989-1992	Authie	256.250	10.220	3.230
1992-1995	Authie	372.207	14.700	3.431
1995-1998	Authie	267.652	9.552	3.422
1998-2001	Authie	219.772	11.246	3.454
2001-2004	Authie	228.932	13.368	3.698
2004-2007	Authie	190.204	11.841	3.777
2007-2010	Authie	211.837	13.306	4.135
2010-2013	Authie	152.272	10.722	4.059
1986-1989	Pirou	343.733	11.161	4.258
1989-1992	Pirou	152.682	8.377	4.360
1992-1995	Pirou	285.144	10.762	4.506
1995-1998	Pirou	175.596	10.294	4.403
1998-2001	Pirou	222.297	9.517	4.465
2001-2004	Pirou	187.057	10.913	4.578
2004-2007	Pirou	233.907	11.234	4.552
2007-2010	Pirou	241.661	8.172	4.610
2010-2013	Pirou	216.044	10.437	4.454
1986-1989	Ay	480.710	6.878	3.055
1989-1992	Ay	254.542	6.245	3.128
1992-1995	Ay	315.653	6.842	3.236
1995-1998	Ay	254.443	6.661	3.248
1998-2001	Ay	220.369	6.246	3.285
2001-2004	Ay	198.295	6.628	3.312
2004-2007	Ay	227.893	6.855	3.268
2007-2010	Ay	228.953	6.610	3.314
2010-2013	Ay	292.531	6.847	3.203
1986-1989	BahiaSanAntonio	6.639	175.112	3.332
1989-1992	BahiaSanAntonio	19.009	188.510	1.191
1992-1995	BahiaSanAntonio	14.242	184.909	1.408
1995-1998	BahiaSanAntonio	9.475	34.713	0.054
1998-2001	BahiaSanAntonio	5.696	170.009	3.908
2001-2004	BahiaSanAntonio	5.590	174.081	4.689
2004-2007	BahiaSanAntonio	6.575	179.405	3.608
2007-2010	BahiaSanAntonio	6.841	171.973	1.114
2010-2013	BahiaSanAntonio	5.981	168.724	1.265
1986-1989	Eureka	22.809	21.045	3.483
1989-1992	Eureka	20.111	18.868	3.292
1992-1995	Eureka	23.693	30.387	2.910
1995-1998	Eureka	17.728	20.133	3.337
1998-2001	Eureka	30.403	22.926	3.489
2001-2004	Eureka	20.835	20.020	3.278
2004-2007	Eureka	13.350	24.595	3.392
2007-2010	Eureka	16.021	22.152	3.808
2010-2013	Eureka	18.262	22.695	3.759
1986-1989	Drakes	20.511	4.248	0.858
1989-1992	Drakes	12.965	3.536	0.936
1992-1995	Drakes	16.045	3.291	0.864
1995-1998	Drakes	58.485	3.328	1.060
1998-2001	Drakes	35.830	2.673	1.008
2001-2004	Drakes	-2.774	2.740	0.927
2004-2007	Drakes	12.384	2.758	0.999
2007-2010	Drakes	11.764	4.522	1.047
2010-2013	Drakes	19.602	3.836	1.081

Period	Estuary	Turbidity	Mudflat	Saltmarsh
1986-1989	EspiritoSanto	145.750	53.495	17.092
1989-1992	EspiritoSanto	134.834	52.356	15.723
1992-1995	EspiritoSanto	149.193	51.693	4.626
1995-1998	EspiritoSanto	169.923	51.634	6.548
1998-2001	EspiritoSanto	158.676	52.100	11.764
2001-2004	EspiritoSanto	160.331	52.202	11.447
2004-2007	EspiritoSanto	102.843	52.582	13.135
2007-2010	EspiritoSanto	73.480	52.648	11.273
2010-2013	EspiritoSanto	129.139	52.689	17.725
1986-1989	Chwaka	72.167	13.482	4.124
1992-1995	Chwaka	93.190	9.172	3.538
1995-1998	Chwaka	70.963	15.560	4.956
1998-2001	Chwaka	284.036	17.102	4.785
2001-2004	Chwaka	129.401	16.677	4.483
2004-2007	Chwaka	97.336	11.939	4.129
2007-2010	Chwaka	203.988	19.097	5.127
2010-2013	Chwaka	71.104	7.968	4.280
1986-1989	Tay	17.517	51.593	6.254
1989-1992	Tay	15.648	43.125	6.822
1992-1995	Tay	92.396	90.174	6.342
1995-1998	Tay	20.703	45.790	6.678
1998-2001	Tay	27.249	53.236	6.259
2001-2004	Tay	21.357	58.174	8.267
2004-2007	Tay	15.933	57.480	5.730
2007-2010	Tay	21.102	58.163	5.973
2010-2013	Tay	13.972	43.352	6.718
1986-1989	Duddon Sands	99.649	25.371	5.347
1989-1992	Duddon Sands	211.183	29.842	5.561
1992-1995	Duddon Sands	249.014	28.148	5.198
1995-1998	Duddon Sands	112.183	27.506	5.361
1998-2001	Duddon Sands	101.529	32.246	5.585
2001-2004	Duddon Sands	136.340	27.570	5.887
2004-2007	Duddon Sands	60.494	30.911	6.279
2007-2010	Duddon Sands	129.717	26.259	6.348
2010-2013	Duddon Sands	38.690	29.537	6.769
1986-1989	Dwyryd	30.584	15.717	6.496
1989-1992	Dwyryd	85.212	15.127	6.651
1992-1995	Dwyryd	207.300	15.701	6.094
1995-1998	Dwyryd	43.114	15.349	6.756
1998-2001	Dwyryd	62.263	13.264	6.546
2001-2004	Dwyryd	23.334	15.087	6.671
2004-2007	Dwyryd	72.548	15.568	6.692
2007-2010	Dwyryd	48.909	15.628	6.838
2010-2013	Dwyryd	71.903	15.410	6.609
1986-1989	Dyfi	138.265	12.950	5.237
1989-1992	Dyfi	182.664	12.242	5.583
1992-1995	Dyfi	313.298	16.381	5.386
1995-1998	Dyfi	38.325	15.469	6.163
1998-2001	Dyfi	136.638	11.653	5.875
2001-2004	Dyfi	22.191	14.886	5.935
2004-2007	Dyfi	105.736	15.073	5.575
2007-2010	Dyfi	64.763	16.245	6.175
2010-2013	Dyfi	89.045	15.253	5.812

Figure A2: The second part of the results of the turbidity and area calculations. This part includes the calculations from Authie to Dyfi. The unit of the mudflat and saltmarsh values are km^2.

Period	Estuary	Turbidity	Mudflat	Saltmarsh
1986-1989	Cleddau Ddu	20.485	18.077	6.595
1989-1992	Cleddau Ddu	18.876	17.157	6.229
1992-1995	Cleddau Ddu	31.514	23.041	6.483
1995-1998	Cleddau Ddu	7.510	18.902	8.327
1998-2001	Cleddau Ddu	16.312	18.739	7.343
2001-2004	Cleddau Ddu	13.182	16.332	7.426
2004-2007	Cleddau Ddu	3.165	18.102	7.634
2007-2010	Cleddau Ddu	16.141	19.725	8.696
2010-2013	Cleddau Ddu	9.275	18.213	6.742
1986-1989	Camel	43.989	6.217	0.872
1989-1992	Camel	29.858	5.444	0.675
1992-1995	Camel	57.881	6.603	0.684
1995-1998	Camel	40.788	6.328	0.854
1998-2001	Camel	37.421	5.433	0.732
2001-2004	Camel	31.699	5.959	0.769
2004-2007	Camel	10.378	6.084	0.778
2007-2010	Camel	50.271	5.821	0.913
2010-2013	Camel	35.973	6.703	0.875
1986-1989	Rogerstown	68.173	4.293	1.355
1989-1992	Rogerstown	68.811	4.281	1.297
1992-1995	Rogerstown	90.067	3.702	1.213
1995-1998	Rogerstown	76.042	4.815	1.340
1998-2001	Rogerstown	86.660	4.457	1.242
2001-2004	Rogerstown	135.382	4.300	1.194
2004-2007	Rogerstown	91.055	4.652	1.186
2007-2010	Rogerstown	116.513	3.302	1.296
2010-2013	Rogerstown	32.645	3.692	1.283
1986-1989	Santander	39.580	4.886	0.873
1989-1992	Santander	38.098	5.085	0.838
1992-1995	Santander	45.261	6.045	0.628
1995-1998	Santander	16.382	5.080	0.674
1998-2001	Santander	22.782	4.844	0.749
2001-2004	Santander	43.035	4.677	0.730
2004-2007	Santander	34.023	5.436	1.102
2007-2010	Santander	23.169	5.184	0.978
2010-2013	Santander	25.492	4.906	1.070
1986-1989	Herbert	216.807	86.814	15.238
1989-1992	Herbert	293.923	99.329	15.854
1992-1995	Herbert	397.014	96.868	13.306
1995-1998	Herbert	351.254	97.865	14.706
1998-2001	Herbert	272.348	97.205	17.096
2001-2004	Herbert	316.580	64.776	12.234
2004-2007	Herbert	270.058	86.038	14.469
2007-2010	Herbert	208.715	86.364	14.414
2010-2013	Herbert	226.937	92.761	17.829
1989-1992	Bombetoka	92.640	241.303	107.604
1992-1995	Bombetoka	115.959	259.541	105.496
1995-1998	Bombetoka	95.178	247.517	116.402
1998-2001	Bombetoka	122.923	246.393	111.877
2001-2004	Bombetoka	147.304	302.574	101.435
2004-2007	Bombetoka	97.015	239.815	98.607
2007-2010	Bombetoka	78.641	231.216	104.116
2010-2013	Bombetoka	86.177	187.352	95.525

Period	Estuary	Turbidity	Mudflat	Saltmarsh
1986-1989	Parnaiba	191.986	180.865	109.149
1989-1992	Parnaiba	212.178	179.173	107.661
1992-1995	Parnaiba	253.865	191.074	99.703
1995-1998	Parnaiba	225.572	192.822	110.655
1998-2001	Parnaiba	217.951	184.221	113.222
2001-2004	Parnaiba	157.024	176.400	115.247
2004-2007	Parnaiba	212.719	176.347	114.970
2007-2010	Parnaiba	224.726	174.389	116.584
2010-2013	Parnaiba	165.451	174.639	117.833
1986-1989	Elbe	116.104	45.419	21.168
1989-1992	Elbe	219.518	47.945	20.849
1992-1995	Elbe	349.795	57.296	20.846
1995-1998	Elbe	197.002	46.871	21.285
1998-2001	Elbe	226.863	44.449	21.482
2001-2004	Elbe	99.737	43.916	21.602
2004-2007	Elbe	176.331	44.703	21.604
2007-2010	Elbe	164.907	44.884	22.055
2010-2013	Elbe	180.616	45.484	21.522
1986-1989	Mottoma	437.066	556.444	93.152
1989-1992	Mottoma	550.782	561.193	57.515
1992-1995	Mottoma	703.677	562.995	53.671
1995-1998	Mottoma	571.816	563.866	46.874
1998-2001	Mottoma	606.843	569.705	47.047
2001-2004	Mottoma	701.194	564.342	71.400
2004-2007	Mottoma	704.995	563.521	13.386
2007-2010	Mottoma	863.381	555.922	12.371
2010-2013	Mottoma	668.602	512.951	11.459
1986-1989	Mubarak	488.998	311.472	0.000
1989-1992	Mubarak	516.431	316.191	0.000
1992-1995	Mubarak	486.339	317.247	0.000
1995-1998	Mubarak	335.344	310.820	0.000
1986-1989	Corubal	334.053	209.598	61.375
1989-1992	Corubal	400.557	153.793	72.415
1992-1995	Corubal	640.197	175.654	31.272
1995-1998	Corubal	315.870	147.398	49.311
1998-2001	Corubal	693.606	187.654	31.581
2004-2007	Corubal	222.719	185.829	76.891
2007-2010	Corubal	414.472	163.288	51.416
2010-2013	Corubal	302.932	166.395	74.516
1986-1989	Willapa	12.615	101.557	17.612
1989-1992	Willapa	8.425	124.995	18.641
1992-1995	Willapa	11.247	111.940	18.922
1995-1998	Willapa	11.619	90.702	21.595
1998-2001	Willapa	8.932	78.994	24.847
2001-2004	Willapa	7.694	144.762	29.799
2004-2007	Willapa	8.909	106.806	24.970
2007-2010	Willapa	9.516	113.942	21.812
2010-2013	Willapa	11.538	69.650	16.738
1986-1989	Nicoya	27.885	71.552	21.234
1989-1992	Nicoya	25.262	70.491	21.089
1992-1995	Nicoya	55.390	37.459	19.247
1995-1998	Nicoya	15.691	54.447	21.606
1998-2001	Nicoya	20.608	70.275	21.542
2001-2004	Nicoya	19.345	43.124	20.923
2007-2010	Nicoya	15.842	40.998	21.906
2010-2013	Nicoya	33.773	75.481	21.490

Figure A3: The third part of the results of the turbidity and area calculations. This part includes the calculations from Cleddau Ddu to Nicoya. The unit of the mudflat and saltmarsh values are km^2.

Period	Estuary	Turbidity	Mudflat	Saltmarsh
1986-1989	Cuna	54.966	78.244	52.686
1989-1992	Cuna	366.252	105.305	46.674
1995-1998	Cuna	31.661	90.058	53.538
1998-2001	Cuna	40.697	65.603	53.151
2001-2004	Cuna	157.114	54.393	33.746
2010-2013	Cuna	7.975	50.163	49.465
1986-1989	Mekong	363.177	53.288	27.573
1989-1992	Mekong	422.529	41.864	25.768
1992-1995	Mekong	351.767	42.188	26.061
1995-1998	Mekong	373.733	57.273	25.211
1998-2001	Mekong	416.781	57.030	24.569
2001-2004	Mekong	529.240	46.396	23.411
2004-2007	Mekong	403.935	45.482	20.285
2007-2010	Mekong	415.857	43.157	20.337
2010-2013	Mekong	334.328	47.597	23.277
1986-1989	Collier	178.216	47.493	10.346
1989-1992	Collier	215.045	46.858	10.132
1992-1995	Collier	190.450	47.959	10.121
1995-1998	Collier	131.153	59.563	11.224
1998-2001	Collier	151.752	51.405	11.421
2001-2004	Collier	210.690	44.386	10.086
2004-2007	Collier	159.252	47.449	11.828
2007-2010	Collier	136.053	48.473	11.976
2010-2013	Collier	196.199	50.410	12.086
2001-2004	Kaipara	31.111	33.972	12.481
2004-2007	Kaipara	35.914	26.068	12.328
2007-2010	Kaipara	63.579	27.585	11.959
2010-2013	Kaipara	27.680	34.924	12.564
1986-1989	Yalujiang	285.270	119.820	0.118
1989-1992	Yalujiang	327.680	125.245	0.014
1992-1995	Yalujiang	409.649	161.729	0.116
1995-1998	Yalujiang	332.701	159.603	0.068
1998-2001	Yalujiang	425.916	134.620	0.017
2001-2004	Yalujiang	352.446	141.994	0.092
2004-2007	Yalujiang	316.848	132.368	9.022
2007-2010	Yalujiang	312.181	116.097	37.368
2010-2013	Yalujiang	305.495	159.683	0.142
1986-1989	Mondego	57.019	10.421	6.025
1989-1992	Mondego	60.570	10.154	5.064
1992-1995	Mondego	217.505	10.803	4.191
1995-1998	Mondego	29.753	11.212	5.633
1998-2001	Mondego	56.640	11.178	5.541
2001-2004	Mondego	-21.308	11.237	6.092
2004-2007	Mondego	51.946	11.054	5.360
2007-2010	Mondego	70.081	10.865	5.853
2010-2013	Mondego	55.783	11.009	5.331
1986-1989	Eems	216.168	3.139	0.065
1989-1992	Eems	189.277	25.420	0.105
1992-1995	Eems	351.131	14.471	0.072
1995-1998	Eems	204.763	20.093	0.085
1998-2001	Eems	207.180	2.355	0.072
2001-2004	Eems	206.648	19.580	0.087
2004-2007	Eems	199.458	6.078	0.087
2007-2010	Eems	140.211	19.968	0.098
2010-2013	Eems	198.042	21.283	0.081
1986-1989	Lawrence	222.456	21.890	5.959
1989-1992	Lawrence	155.206	25.541	8.022
1992-1995	Lawrence	298.095	20.819	3.563
1995-1998	Lawrence	168.900	26.797	8.906
1998-2001	Lawrence	182.658	30.814	8.308
2001-2004	Lawrence	172.839	22.380	6.896
2004-2007	Lawrence	194.797	23.146	8.188
2007-2010	Lawrence	196.501	29.581	8.292
2010-2013	Lawrence	165.825	25.504	8.732

Figure A4: The fourth part of the results of the turbidity and area calculations. This part includes the calculations from Cuna to Lawrence. The unit of the mudflat and saltmarsh values are km^2.

Westerschelde	+		Dyfi	-
Oosterschelde	+		Cleddau Ddu	-
Arcachon	-		Camel	+
Blackwater	+		Rogerstown	±
Colne	+		Santander	+
Humber	+		Herbert	-
Eden	-		Bombetoka	x
Olhao	±		Parnaiba	-
Exe	+		Elbe	±
Plymouth	+		Mottoma	+
SaintMichel	-		Mubarak	x
Medway	±		Corubal	-
Authie	-		Willapa	+
Pirou	±		Nicoya	-
Ay	-		Cuna	x
BahiaSanAntonio	x		Mekong	-
Eureka	±		Collier	±
Drakes	-		Kaipara	x
EspiritoSanto	-		Yalujiang	+
Chwaka	-		Mondego	-
Tay	-		Eems	+
Duddon Sands	-		Lawrence	+
Dwyryd	-			

Figure A5: The results of the hypsometric tool for all estuaries. Green = accreting, red = eroding, yellow = stable and grey = not sufficient data available.

AOI	Std	Range	Median	High Turbidity	Trend
Westerschelde	41.92	138.67	103.03	TRUE	-
Oosterschelde	16.70	46.99	22.41	FALSE	-
Arcachon	5.02	16.09	16.04	FALSE	-
Blackwater	66.88	231.82	88.94	TRUE	-
Colne	50.19	167.90	172.80	TRUE	-
Humber	39.90	136.64	210.60	TRUE	-
Eden	15.80	50.26	17.63	FALSE	-
Olhao	19.10	61.18	52.97	TRUE	+
Exe	47.24	124.75	55.32	TRUE	-
Plymouth	12.01	42.25	12.85	FALSE	-
SaintMichel	31.88	96.39	111.73	TRUE	+
Medway	58.84	188.36	102.07	TRUE	-
Authie	62.35	219.93	219.77	TRUE	-
Pirou	58.25	191.05	222.30	TRUE	-
Ay	85.39	282.42	254.44	TRUE	-
BahiaSanAntonio	4.68	13.42	6.64	FALSE	-
Eureka	4.97	17.05	20.11	FALSE	-
Drakes	17.46	61.26	16.04	FALSE	-
EspiritoSanto	30.79	96.44	145.75	TRUE	-
Chwaka	77.35	213.07	95.26	TRUE	-
Tay	24.73	78.42	20.70	FALSE	+
Duddon Sands	66.99	210.32	112.18	TRUE	-
Dwyryd	54.80	183.97	62.26	TRUE	-
Dyfi	88.27	291.11	105.74	TRUE	-
Cleddau Ddu	8.31	28.35	16.14	FALSE	-
Camel	13.52	47.50	37.42	TRUE	-
Rogerstown	29.50	102.74	86.66	TRUE	+
Santander	10.28	28.88	34.02	TRUE	-
Herbert	63.47	188.30	272.35	TRUE	-
Bombetoka	22.65	68.66	96.10	TRUE	-
Parnaiba	30.59	96.84	212.72	TRUE	-
Elbe	72.70	250.06	180.62	TRUE	-
Mottoma	121.13	426.31	668.60	TRUE	+
Mubarak	82.09	181.09	487.67	TRUE	-
Corubal	166.67	470.89	367.30	TRUE	-
Willapa	1.72	4.92	9.52	FALSE	-
Nicoya	13.13	39.70	22.93	FALSE	-
Cuna	135.84	358.28	47.83	TRUE	-
Mekong	57.48	194.91	403.93	TRUE	+
Collier	31.22	83.89	178.22	TRUE	-
Kaipara	16.36	35.90	33.51	TRUE	
Yalujiang	47.54	140.65	327.68	TRUE	-
Mondego	63.62	238.81	56.64	TRUE	-
Eems	56.46	210.92	204.76	TRUE	-
Lawrence	43.51	142.89	182.66	TRUE	-

Figure A6: The standard deviation, range and median of the turbidity values of each estuary is shown, as well as whether or not an estuary can be considered to have high turbidity and the trend of the turbidity over time.

AOI	Correlation	P-Value	AOI	Correlation	P-Value
Westerschelde	-0.5833	0.0992	Dyfi	-0.7833	0.0125
Oosterschelde	-0.5667	0.1116	Cleddau Ddu	-0.7000	0.0358
Arcachon	-0.3000	0.4328	Camel	0.2667	0.4879
Blackwater	-0.2000	0.6059	Rogerstown	-0.6333	0.0671
Colne	-0.8000	0.0096	Santander	-0.2000	0.6059
Humber	-0.5667	0.1116	Herbert	-0.3333	0.3807
Eden	-0.2833	0.4600	Bombetoka	0.1667	0.6932
Olhao	-0.1500	0.7001	Parnaiba	-0.4333	0.2440
Exe	-0.1167	0.7650	Elbe	-0.6000	0.0876
Plymouth	-0.2833	0.4600	Mottoma	-0.5500	0.1250
SaintMichel	-0.0833	0.8312	Mubarak		
Medway	-0.6000	0.0876	Corubal	-0.8095	0.0149
Authie	-0.5500	0.1250	Willapa	-0.6500	0.0581
Pirou	0.1667	0.6682	Nicoya	-0.6429	0.0856
Ay	-0.8333	0.0053	Cuna	-0.6000	0.2080
BahiaSanAntonio	-0.7333	0.0246	Mekong	-0.1833	0.6368
Eureka	-0.3000	0.4328	Collier	-0.4667	0.2054
Drakes	0.2333	0.5457	Kaipara	-1.0000	0.0000
EspiritoSanto	-0.4000	0.2861	Yalujiang	-0.6167	0.0769
Chwaka	0.2857	0.4927	Mondego	-0.4667	0.2054
Tay	-0.0833	0.8312	Eems	-0.8167	0.0072
Duddon Sands	-0.5000	0.1705	Lawrence	-0.5667	0.1116
Dwyryd	-0.3000	0.4328			

Figure A7: The correlation and corresponding p-values between turbidity change and saltmarsh area change for all estuaries in this study. AOI = Area of interest, in this case the name of the estuary.

AOI	Positive	Negative	Error / No change
Westerschelde		x	
Oosterschelde		x	
Arcachon	x		
Blackwater		x	
Colne		x	
Humber		x	
Eden	x		
Olhao			x
Exe		x	
Plymouth		x	
SaintMichel		x	
Medway			x
Authie	x		
Pirou		x	
Ay	x		
BahiaSanAntonio			x
Eureka			x
Drakes	x		
EspiritoSanto	x		
Chwaka		x	
Tay	x		
Duddon Sands	x		
Dwyryd	x		
Dyfi	x		
Cleddau Ddu	x		
Camel		x	
Rogerstown			x
Santander		x	
Herbert	x		
Bombetoka			x
Parnaiba	x		
Elbe			x
Mottoma	x		
Mubarak			x
Corubal	x		
Willapa		x	
Nicoya	x		
Cuna			x
Mekong		x	
Collier			x
Kaipara			x
Yalujiang		x	
Mondego	x		
Eems		x	
Lawrence		x	
Total	17	17	11
Percentage	38%	38%	24%

Figure A8: The simple correlation between turbidity change and whether a saltmarsh is accreting or eroding based on the hypsometric curve. AOI = Area of interest, in this case the name of the estuary.

AOI	1986-1989	1989-1992	1992-1995	1995-1998	1998-2001	2001-2004	2004-2007	2007-2010	2010-2013
Westerschelde	35	40	37	41	31	18	41	29	27
Oosterschelde	35	40	37	38	31	18	33	28	27
Arcachon	29	29	27	56	35	17	32	25	23
Blackwater	29	41	31	41	30	20	41	27	24
Colne	29	41	31	41	30	20	41	27	24
Humber	46	72	61	73	54	32	57	37	31
Eden	29	32	42	67	41	22	34	29	26
Olhao	41	34	52	51	44	23	33	38	23
Exe	40	44	43	38	41	19	34	35	20
Plymouth	40	44	43	38	41	19	34	35	20
SaintMichel	31	40	41	53	34	23	28	30	20
Medway	29	41	31	41	30	20	41	27	24
Authie	31	47	38	32	24	22	34	30	28
Pirou	31	40	41	53	34	23	28	30	20
Ay	31	40	41	53	34	23	28	30	20
BahiaSanAntonio	39	4	4	1	44	51	102	65	33
Eureka	25	27	37	41	27	34	35	36	22
Drakes	111	91	112	80	78	102	120	111	71
EspiritoSanto	10	54	37	48	45	12	40	34	8
Chwaka	10	0	4	22	11	4	18	15	8
Tay	35	41	55	67	61	27	38	38	38
Duddon Sands	24	27	39	32	24	10	33	22	28
Dwyryd	28	33	35	27	29	14	27	21	25
Dyfi	27	36	42	31	36	18	29	21	25
Cleddau Ddu	37	39	27	29	35	19	40	25	22
Camel	21	23	19	22	30	16	23	18	13
Rogerstown	23	25	20	22	26	11	28	19	26
Santander	41	52	52	71	55	32	46	43	34
Herbert	53	83	112	91	63	20	107	72	50
Bombetoka	0	17	19	31	27	6	23	19	6
Parnaiba	31	28	17	3	25	28	46	42	10
Elbe	57	80	75	62	68	38	83	44	43
Mottoma	8	32	32	37	37	9	28	33	13
Mubarak	114	146	141	164					
Corubal	19	13	5	9	4	0	5	25	14
Willapa	59	47	57	50	47	67	78	61	40
Nicoya	30	21	2	28	51	6	0	4	3
Cuna	11	7	0	7					
Mekong	13	43	45	68	62	21	58	58	16
Collier	34	56	66	67	43	15	96	91	34
Kaipara	0	0	0	0	0	7	32	8	10
Yalujiang	27	33	40	36	33	33	40	28	20
Mondego	35	38	44	49	38	18	41	31	15
Eems	34	32	25	29	29	17	34	25	21
Lawrence	82	70	78	60	51	63	90	79	51
Mean	**33**	**38.837209**	**39.44186**	**42.534884**	**37.511628**	**23.651163**	**43.697674**	**35.930233**	**24.55814**

Figure A9: The image count per estuary per period is shown in this figure. The mean number of images per period is shown at the bottom.

Appendix B

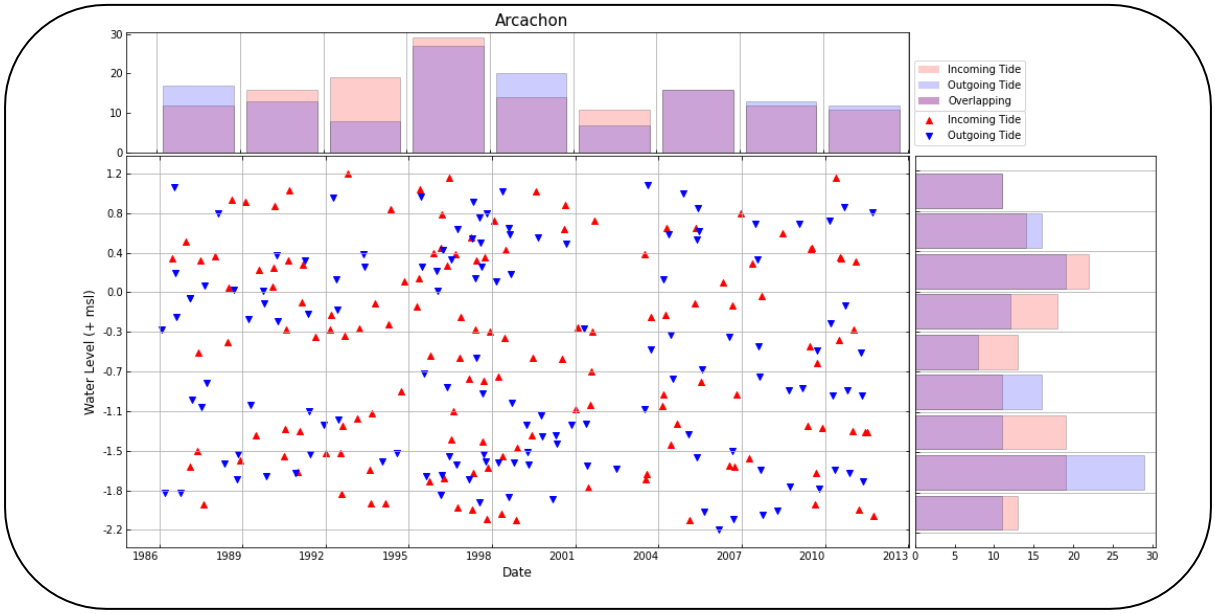

Figure B1: Index of dispersion for Arcachon, showing the date and the tide. Each datapoint has a collection date and an associated tide with it.

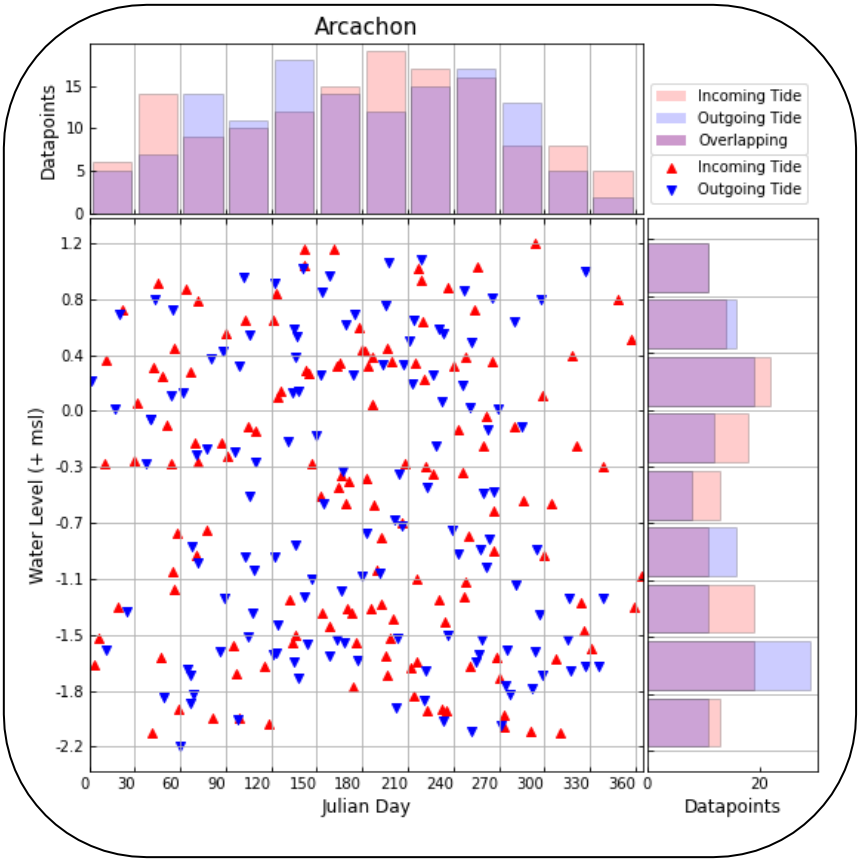

Figure B2: Index of dispersion for Arcachon, showing the Julian Day and the tide. Each datapoint is an image and shows the Julian day it was taken on and the tide level at that time.

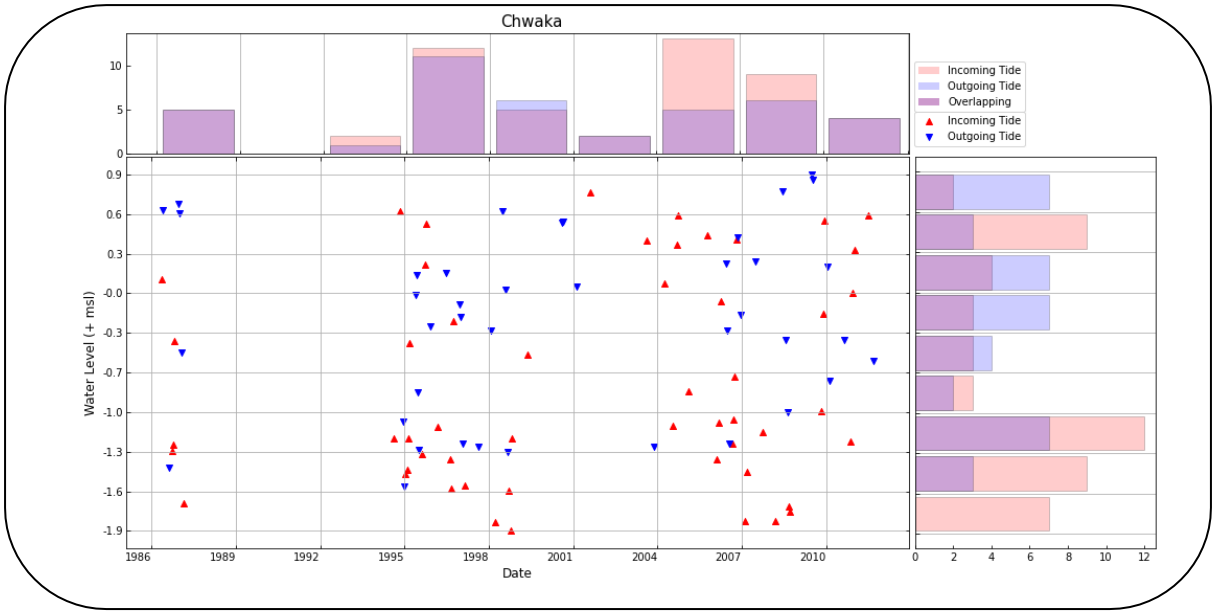

Figure B3: Index of dispersion for Chwaka, showing the date and the tide. Each datapoint has a collection date and an associated tide with it.

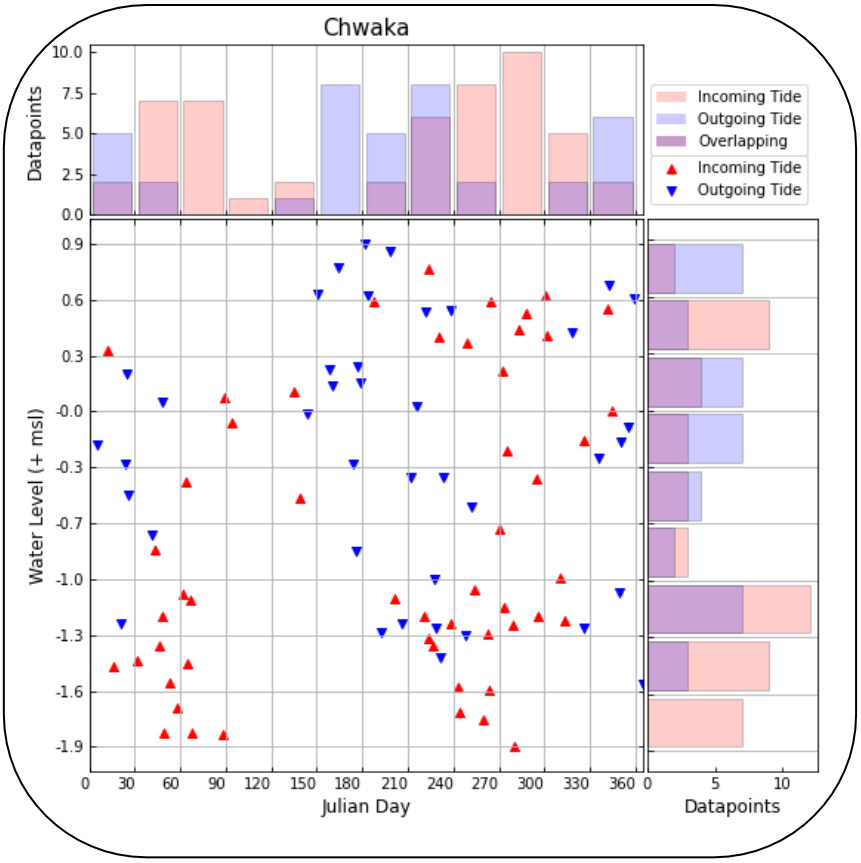

Figure B4: Index of dispersion for Chwaka, showing the Julian Day and the tide. Each datapoint is an image and shows the Julian day it was taken on and the tide level at that time.

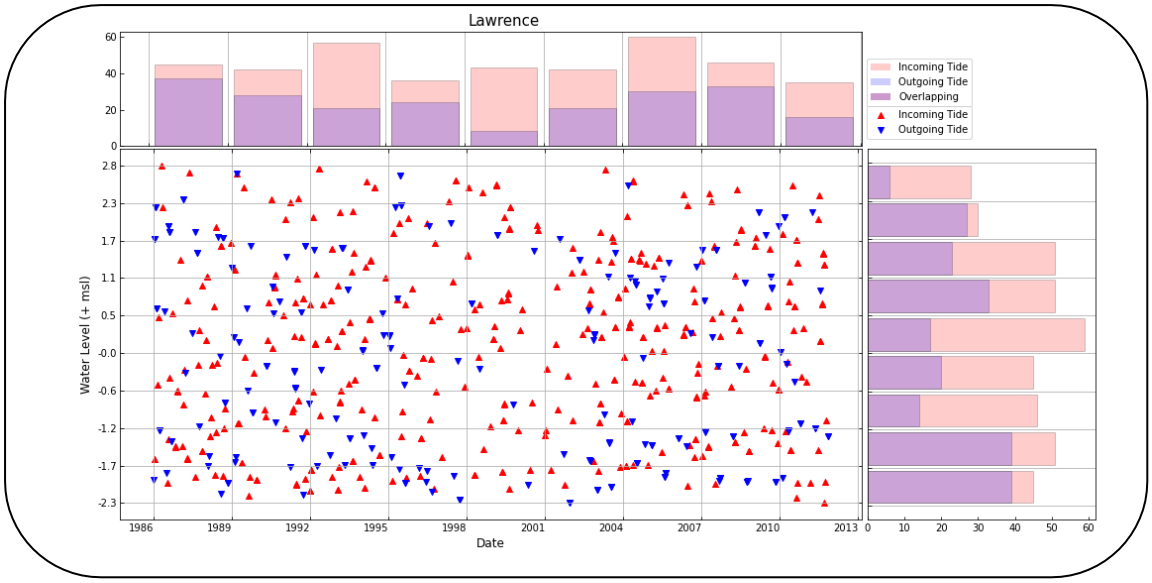

Figure B5: Index of dispersion for Lawrence, showing the date and the tide. Each datapoint has a collection date and an associated tide with it.

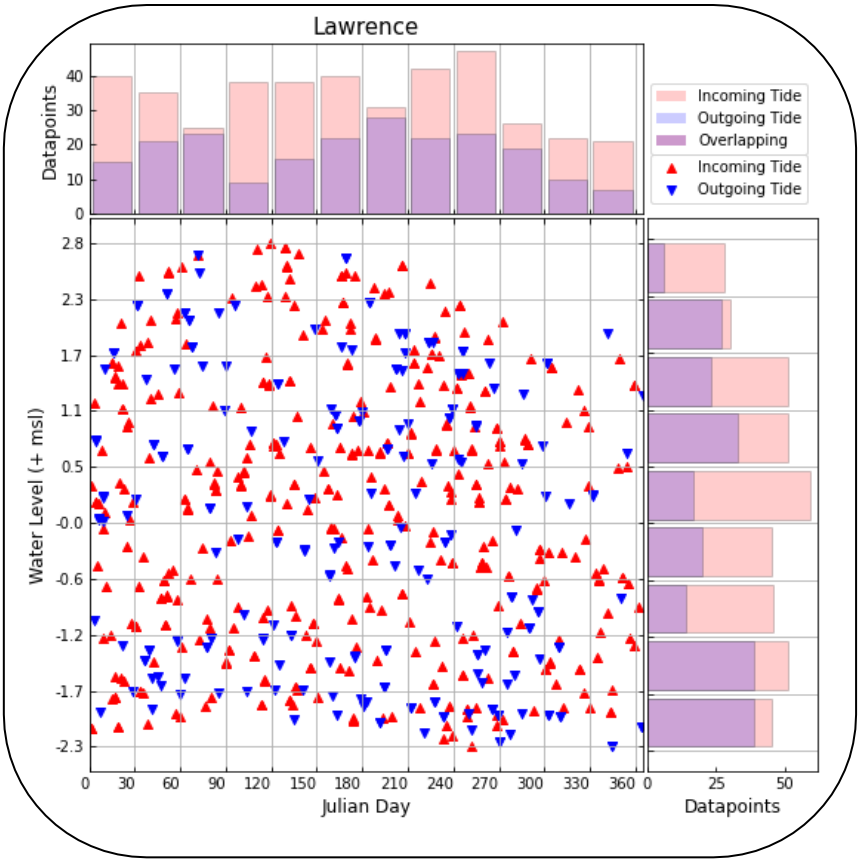

Figure B6: Index of dispersion for Lawrence, showing the Julian Day and the tide. Each datapoint is an image and shows the Julian day it was taken on and the tide level at that time.

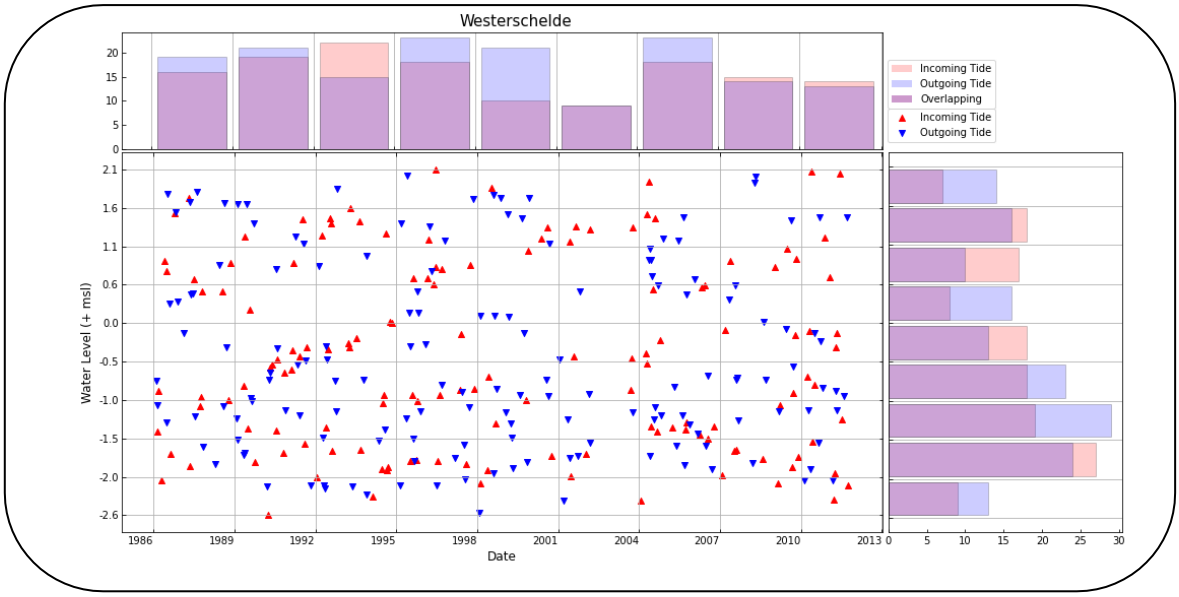

Figure B7: Index of dispersion for Westerschelde, showing the date and the tide. Each datapoint has a collection date and an associated tide with it.

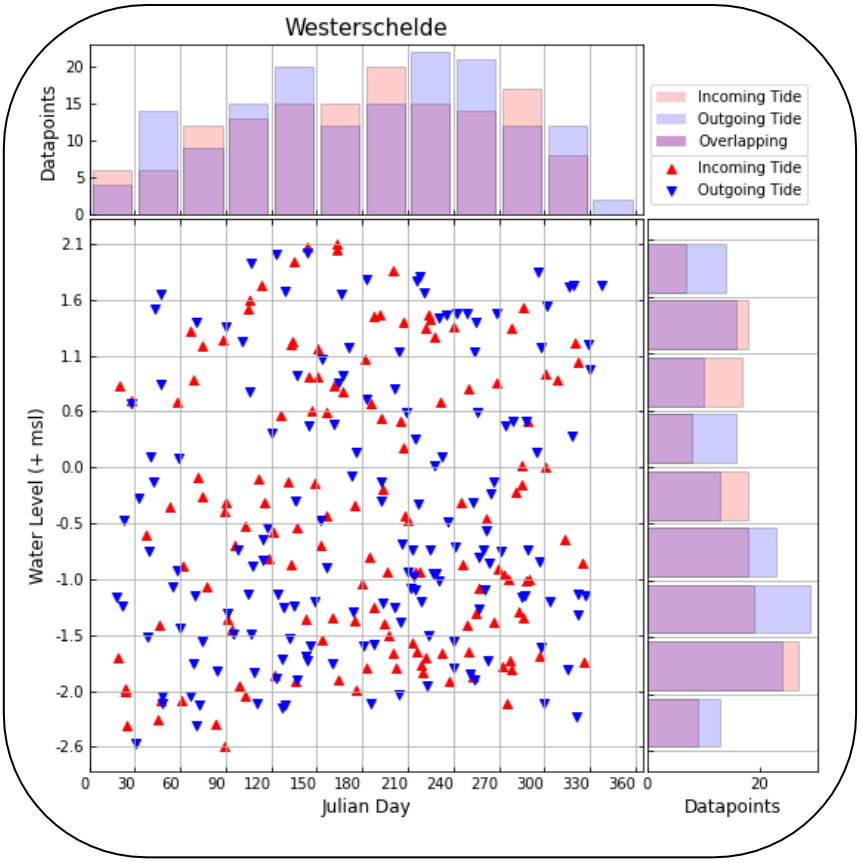

Figure B8: Index of dispersion for Westerschelde, showing the Julian Day and the tide. Each datapoint is an image and shows the Julian day it was taken on and the tide level at that time.

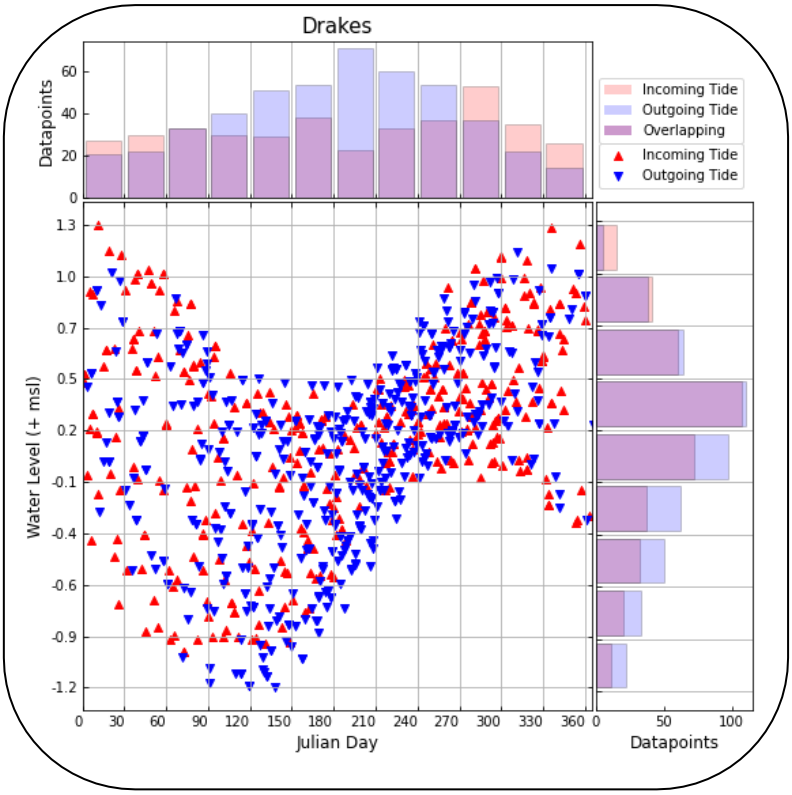

Figure B9: Index of dispersion for Drakes, showing the Julian Day and the tide. Each datapoint is an image and shows the Julian day it was taken on and the tide level at that time. This index of dispersion shows significant clustering.

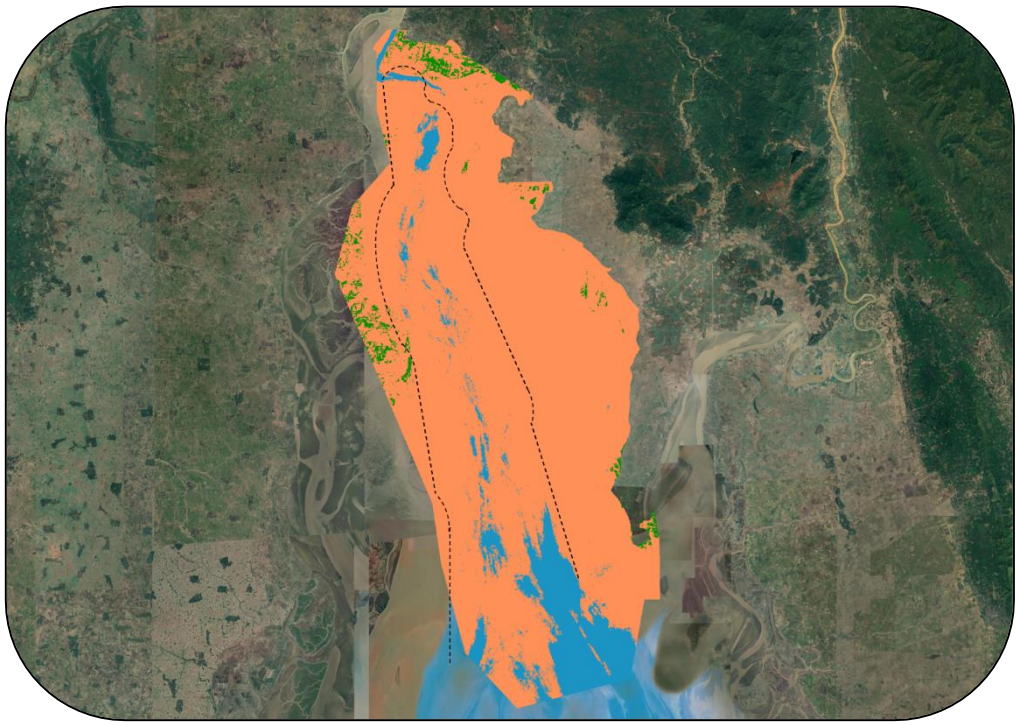

Figure B10: The Mottoma Estuary, located in the gulf of Mottoma / The gulf of Martaban, Myanmar. This highly turbid estuary shows a wrongly classified mudflat area. The black dotted line shows the approximate area of the water channel.

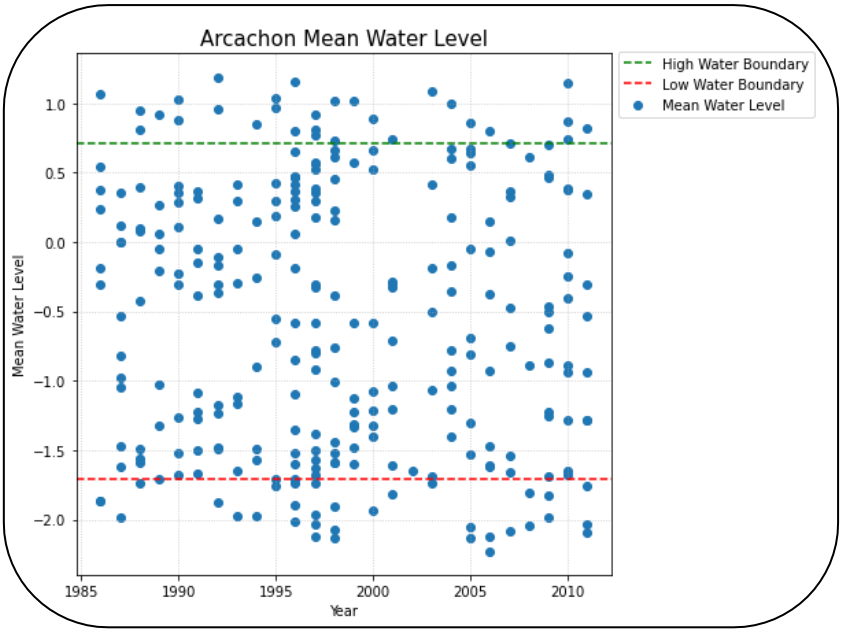

Figure B11: The water level for each datapoint is shown. The high-water boundary (green line) is based on the minimum of the maximum water level per period. The low-water boundary (red line) is based on the maximum of the minimum water level per period.